FINITE ELEMENT MODELING OF A PIEZO PATCH ENERGY HARVESTER AND EQUIVALENT CIRCUIT MODELING ON A THIN PLATE WITH AC-DC CONVERSION

by

Buğra Bayık

A Thesis Submitted to the
Graduate School of Engineering
in Partial Fulfillment of the Requirements for
the Degree of

Master of Science
in
Mechanical Engineering

January 2016
Koc University
Graduate School of Sciences and Engineering

This is to certify that I have examined this copy of a master's thesis by

Buğra Bayık

and have found that it is complete and satisfactory in all respects,
and that any and all revisions required by the final
examining committee have been made.

Committee Members:

____

Ipek Basdogan, Ph. D.

____

Murat Sözer, Ph. D.

____

Kenan Şanlıtürk, Ph. D.

Date: ______________________________

ABSTRACT

Research on vibration based energy harvesting has received great interest over the last two decades with motivation to provide continuous power to small electronic devices and eliminate the need of battery replacement and disposal. Ambient vibrations available in the environment of such devices can be converted to electric energy through piezoelectric transduction mechanisms. A typical piezoelectric energy harvester application is attachment of a cantilever beam with piezoceramic layers to a vibrating host structure. Energy harvesting circuits are connected to piezoceramic layers to convert the AC output of the harvesters into a stable DC output to charge storage components. Cantilever harvesters have been widely studied in the literature.

As an alternative to beam harvesters, piezoelectric patches can be easily integrated to thin plates to extract vibrational energy of their host structure and convert it into electrical energy. This implementation can be convenient especially for thin structures employed in aerospace, automotive, and marine applications to enable compact and broadband energy harvesting. Integrating piezo-patch energy harvesters to such host plates eliminates the mass loading and volumetric occupancy of base-excited cantilever design. Relatively limited literature has focused on energy harvesting for those two-dimensional structures.

In this thesis, first, a coupled electroelastic FE model of a patch based piezoelectric energy harvester integrated to a thin plate is generated. Then, a multi-mode equivalent circuit model of the piezo-patch energy harvester is developed using finite-element model of the harvester by accounting for two-way coupling. Multi-mode circuit representation of the harvester is connected to linear and nonlinear circuit elements using the SPICE software. Simulation results are validated for the standard AC-AC and AC-DC configurations. For the AC input – AC output problem, voltage frequency response functions are calculated for various resistive loads, and they show excellent agreement with modal analysis-based analytical closed-form solution and with the finite-element model. For the AC input – DC output case, a full-wave rectifier and a smoothing capacitor are connected to the harvester circuit for conversion of the AC voltage to stable DC voltage.

Finally, FE modeling technique for the AC input-AC output problem is also demonstrated on a case study which involved harvesting on a vibrating panel of a heavy duty truck cabin. The vibration response of the panel as well as the voltage output of the harvester patch under the real operating conditions is simulated using the forces obtained from experimental measurements on the vehicle. The electrical power generation of the harvester patch is predicted for a wide range of resistive loads. Electrical power outputs are then presented for short-circuit and open-circuit conditions. The numerical results show that the use of a harvester patch attached on a panel of a heavy duty vehicle generates reasonably good electrical power outputs.

ÖZET

Küçük elektronik cihazlara sürekli güç kaynağı sağlayabilmek amacıyla, titreşim tabanlı piezoelektrik enerji hasadı, araştırmacılar tarafından yoğun ilgi görmektedir. Piezoelektrik enerji hasadıyla ilgili en yaygın uygulama, piezoseramik katmanla örtülü ankastre kirişin titreşen ana yapıya bağlanmasıdır. Piezoseramik katmana bağlanan elektrik devresi AC çıktıyı kararlı DC çıktısına dönüştürür ve depolama bileşeninin şarj edilmesini sağlar. Literatürde yaygın olarak bahsedilen kiriş yapıda enerji üreteçleri çalışılmıştır.

Piezoseramik yamaların doğrudan ince plaka benzeri yapılara entegre edildiği uygulamalar ise kiriş yapıdaki üreteçlere alternatif olarak kullanılabilir. Bu yöntem özellikle havacılık, otomotiv ve denizcilik uygulamalarında, ince plaka benzeri yapılarda kompakt ve geniş bantlı enerji hasadı imkânı sağlayacaktır. Ancak, literatürde iki boyutlu yapılarda enerji hasadı uygulamaları, kiriş yapılardaki uygulamalara göre kısıtlıdır.

Bu tezde ilk olarak, ince plaka şeklindeki ana yapıya bağlı piezoseramik yama için elektro-elastik sonlu elemanlar modeli oluşturulmuştur. Daha sonra sonlu elemanlar modeli kullanılarak çok modlu eşdeğer devre modeli elde edilmiştir. Enerji üretecinin çok modlu eşdeğer devre modeline, SPICE yazılımında, lineer ve lineer olmayan enerji hasadı devreleri eklenmiştir. Simülasyon sonuçları lineer AC-AC ve lineer olmayan AC-DC devre konfigürasyonları için doğrulanmıştır. AC-AC konfigürasyonu için voltaj frekans cevap fonksiyonları, farklı direnç yükleri bağlanarak hesaplanmış ve sonuçlar kapalı yapıdaki analitik model ve sonlu elemanlar modeli sonuçlarıyla karşılaştırılmıştır. Sonuçlar arasında çok yüksek benzerlik görülmüştür. AC-DC konfigürasyonunda, kararlı bir doğru akım voltajı elde edebilmek için, tam dalgalı doğrultucu ve süzgeçleme kapasitörü kullanılmıştır.

Son olarak, sonlu elemanlar modeli ile ilgili bir vaka çalışması yapılmış, ve ana yapı olarak ağır yük kamyonu kabininin titreşen paneli kullanılmıştır. Deneysel verilerden elde edilen kuvvetler kullanılarak, operasyonel koşullar altında panelin titreşim cevabı ve panele entegre edilen piezoseramik yamanın voltaj cevabı elde edilmiştir. Kapalı devre ve açık devre koşullarında elektrik gücü çıktıları sunulmuştur. Nümerik sonuçlar elektrik gücü çıktılarının kabul edilebilir düzeyde olduğunu göstermektedir.

ACKNOWLEDGEMENTS

Foremost, I am sincerely grateful to my supervisor Assoc. Prof. Ipek Başdoğan who offered invaluable guidance and encouragement during this thesis. I appreciate all her contributions of ideas and support to make my research experience productive. Besides my advisor, I consider it an honor to acknowledge Asst. Prof. Alper Erturk for his insightful comments which helped me to improve my research to a more contributive and enjoyable level. I would like to thank my thesis committee members Prof. Kenan Y. Şanlıtürk and Assoc. Prof. Murat Sözer for their comprehensive review of my work.

My sincere gratitude goes to Dr. Uğur Arıdoğan for his valuable comments, collaboration and encouragement. I am also very grateful to Amirreza Aghakhani for his close collaboration and support to overcome the difficulties I have encountered at crucial steps of my thesis. I am very thankful to all my good friends and lab mates Andrei Christian Stan, Hakan Yenerer, Utku Boz, Gökhan Serhat, Mehmet Murat Gözüm, Egemen Aşkın and Hakan Uçar for providing very friendly and productive environment to keep my motivation higher.

Last but not least, I thank my brother and my parents for their support and patience.

TABLE OF CONTENTS

LIST OF FIGURES

LIST OF TABLES

NOMENCLATURE

a	Length of the host structure
b	Width of the host structure
c_{ijkl}	Elastic stiffness constant
C_{mn}	Equivalent capacitance
C_p	Capacitance of the piezoceramic patch
C_u	Damping matrix
C_v	Damping permittivity matrix
D_i	Electric displacement component
d_{ijk}	Piezoelectric constant
E_i	Electric field component
e_{ijk}	Piezoelectric constant
F	Nodal force vector
f	Transverse point force
F_0	Amplitude of the transverse force
H	Heaviside functions
h_p	Thickness of the piezoceramic patch
h_s	Thickness of the host structure
i_{mn}	Electrical current of the equivalent circuit
K^u	Stiffness matrix
K^z	Off-diagonal stiffness submatrices
L	electric charge vector

L_{mn}	Equivalent inductance
l_p	Length of the piezoceramic patch
M	Mass matrix
N_{mn}	Ideal transformer ratio
q_{mn}	Electrical charge of the equivalent circuit
R_l	Resistive load
R_{mn}	Equivalent resistance
S_{ij}	Strain component
s_{ijkl}	Elastic compliance constant
T_{ij}	Stress component
u	Nodal displacement vector
V	Electric potential vector
v	Voltage across the resistive load
V_c	Rectified voltage
V_{mn}	Equivalent voltage source
w	Transverse deflection of the host plate
w_p	Width of the piezoceramic patch
x_0	x-coordinate of transverse point force
x_1	x-coordinate of left corner of the piezoceramic patch
x_2	x-coordinate of right corner the piezoceramic patch
y_0	y-coordinate of transverse point force
y_1	y-coordinate of left corner of the piezoceramic patch
y_2	y-coordinate of right corner of the piezoceramic patch

Y_s	Young's modulus
ε	Permittivity component
θ	Electromechanical coupling term
v	Poisson's ratio
ρ	Density

Chapter 1

INTRODUCTION

1.1. Vibration Based Energy Harvesting with Piezoelectric Transduction

Research on vibration based energy harvesting has received great interest over the last two decades with motivation to provide continuous power to small electronic devices and eliminate the need of battery replacement and disposal. Ambient vibrations available in the environment of such devices can be converted to electric energy through electrostatic [1, 2], electromagnetic [3, 4] and piezoelectric transduction mechanisms [5, 6].

Using piezoelectric transduction, energy conversion from ambient vibrations to electric energy occurs due to direct piezoelectric effect. Direct piezoelectric effect is simply generation of electrical charge on faces of piezoelectric material resulting from applied strain energy. In energy harvesting applications, "direct piezoelectric effect" and "converse piezoelectric effect" may exist at the same time. Converse piezoelectric effect is deformation of piezoelectric material due to applied voltage across faces of piezoelectric material. Direct piezoelectric effect of piezoelectric materials is used in many sensor applications. Piezoelectric shunt damping applications are also based on direct piezoelectric effect but the charge output of the piezoelectric material is dissipated for damping purpose rather than sensing or energy harvesting.

In electromagnetic transduction, oscillatory motion of a magnet in a coil causes current to flow in coil [7-9], while electrostatic transduction is achieved by relative motion of two conductors separated by a dielectric (i.e. a capacitor) [10]. Motion of the conductors changes the energy stored in the capacitor and results in mechanical to electrical energy conversion. Among basic transduction mechanisms, piezoelectric energy harvesters have drawn the greatest attention mainly due to their large power densities. Power densities of piezoelectric materials are comparable to thin-film and thick-film lithium ion batteries and thermoelectric generators [11]. Compared to electromagnetic devices, voltage output of piezoelectric devices are higher and can be directly used to charge the storage components while electromagnetic devices require additional post processing to reach the required voltage output level [12]. Another advantage of piezoelectric devices over electromagnetic devices is their ease of fabrication for small scale applications [13, 14]. The main disadvantage of electrostatic converters is requirement of an additional voltage source to initiate the energy conversion [15].

The most common application of piezoelectric energy harvesting includes a cantilever beam covered by one or two layers of piezoelectric materials, referred as unimorph and bimorph configurations respectively. Harvester beams are attached to vibrating host structures and alternating voltage output is obtained across the electrodes of the harvester. In practice, alternating voltage output must be converted to constant voltage output with an AC-DC rectifier followed by a smoothing capacitor. However, in mathematical models of energy harvesters and most experimental studies, harvesting circuits are simply represented by a resistive load [14, 16-21] which is sufficient to investigate achievable power output of an energy harvester.

Another application of piezoelectric energy harvesting is attachment of a piezoceramic patch directly to a vibrating host structure. This application is referred as patch based energy harvester in this study. Compared to cantilever beam harvesters, patch based energy harvesters have several advantages. Lee et al. [22] listed the main drawbacks of cantilever beam harvesters as requirement of extra space for proof mass and clamping mechanism, energy loss due to loosened clamping condition of the beam and need of housing for protection of the energy harvester from environmental harms. Compared to cantilever beams, compact and lightweight patch based energy harvesters on a vibrating host structure can be designed since a housing covering a large proof mass or a clamping mechanism is not needed. In addition, broadband energy harvesting capabilities of patch based energy harvesters are higher due to closely separated vibration modes compared to cantilever beams. A broadband patch based energy harvesting application, utilizing closely separated vibration modes of plate-like sturctures, is studied by Aridogan et al. [23] by combining electrical outputs of multiple patches from several vibration modes of the host structure into a single electrical output. A typical patch based harvester attached to a plate structure is shown in Figure 1.

a) b)

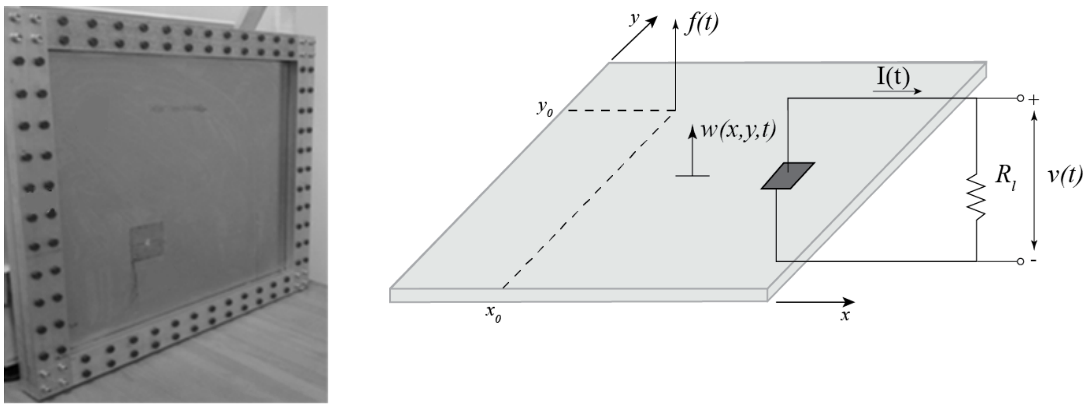

Figure 1. a) Patch based piezoelectric energy harvester attached on a fully clamped plate. b) Schematic view of the harvester with the resistive load

1.2. Review of Mathematical Models of Piezoelectric Energy Harvesters

Objective of mathematical modeling of piezoelectric energy harvesters is to estimate voltage output of the harvesters across the attached resistive load and obtain the delivered power. Studies on piezoelectric energy harvesting can be focused on mechanics of vibration, electric circuitry or behavior of piezoelectric materials. Therefore, researchers from different disciplines studied the piezoelectric energy harvesting problem and various approaches have been developed.

Erturk and Inman [24] provided a summary of issues regarding the existing electromechanical models of piezoelectric energy harvesters along with necessary corrections and clarifications on oversimplified and incorrect physical assumptions.

In an early work on vibration based energy harvesting, Williams and Yates [25] developed a lumped-parameter model and obtained power output of an energy harvester based on electromagnetic transduction. They included the backward coupling of the electrical domain as an additional viscous damping term in the mechanical domain, assuming that backward coupling is only proportional to velocity. Although this assumption is valid for electromagnetic energy harvesters, (i.e. oscillatory motion of a seismic magnetic mass in a coil) it does not apply to piezoelectric coupling. In the literature, some SDOF models for piezoelectric energy harvesters are based on this assumption and use of these models result in incorrect estimations of voltage and power outputs. Existing incorrect SDOF modeling approaches, which assume backward coupling is proportional to velocity, are discussed in the study by Erturk and Inman [24].

Another lumped parameter model was introduced by duTouit et al which takes into account the backward coupling in a more complicated way [26]. Authors used the longitudinal mode of the piezoelectric material, rather than the typical bending mode used in cantilever beam harvesters. In the model by duToit, correct modeling of backward coupling allows the prediction of short circuit and open circuit trends which can not be observed using viscous damping assumption. Authors show that, as the resistive load increases from zero to infinity (i.e. from short circuit condition to open circuit condition) resonance frequency of the harvester increases.

A SDOF model which takes into account the backward electrical coupling is introduced by Roundy et al for a cantilever beam harvester working in bending mode [17]. Authors neglected the distributed mass of the cantilever beam and included a large tip mass in the model. However, neglecting the distributed mass of the cantilever beam may result in inaccurate estimation of natural frequency and excitation force. Erturk and Inman [27] proposed correction factors for excitation amplitudes which depend on proof mass to beam mass ratio.

As an improvement to above mentioned lumped parameter models, which neglect the distributed mass of the cantilevered harvester, Rayleigh-Ritz formulation is used by Sodano and DuToit [26, 28-32]. The Rayleigh–Ritz model is an approximate representation of the distributed parameter system and computationally more expensive than analytical models. Computationally more efficient exact analytical solutions for a cantilevered piezoelectric energy harvester are given by Erturk and Inman [19, 20] with experimental validations. Since the ambient vibrations are frequency dependent or totally random in practice, numerous studies focused on broadening the bandwidth of cantilever harvesters. New configurations were proposed by building mechanical band-pass filters with array of beams [33], adding nonlinearities with compressive axial preload configurations [34, 35], attaching movable tip masses [36], coupling with electromagnetics [37, 38] and mechanically stiffening structures [39] for improving the performance of the beam harvesters.

Plate-like harvesters are good alternatives to cantilever beam harvesters. However, compared to the number of studies dealing with piezoelectric harvester beams, research on plate-like piezoelectric energy harvesters has been very limited. De Marqui et al [40] presented electromechanically coupled FE model for a piezoelectric energy harvester plate, and later on extended this model by including piezoaeroelastic coupling to analysis of an energy harvester embedded on a plate-like wing [41, 42]. Rupp et al [43], designed multilayer piezoelectric energy harvester system composed of structural, mechanical and piezoelectric layers and conducted a topology optimization study to maximize harvested power output. An analytical model was presented by Harne et al [44] representing coupled electroelastic dynamics of distributed energy harvesting device, corrugated piezoelectric spring, attached on a panel. Harne further analyzed this device to show vibration control and energy harvesting potentials and challenges of superposing vibration control and energy harvesting goals [45]. More recently, Aridogan et al. [21], have presented analytical closed-form expressions and experimental validations of patch-based piezoelectric energy harvesters structurally integrated to fully clamped plates.

In modelling of both cantilever beam and plate-like harvesters, usually a simple resistive load is used to estimate power outputs [20, 21]. However, practical energy harvesters require more complex interface circuits to provide a stable DC signal for storage devices. A standard practical circuit includes a rectifier bridge as an AC-DC converter followed by a smoothing capacitor [46-48]. Ottman et al suggested using a DC-DC converter right after the AC-DC converter to maximize power transfer to the storage device through impedance matching [47]. Later synchronized switch harvesting on inductor (SSHI) technique is suggested to boost up power output of the energy harvesters [48-50].

Simulation of piezoelectric energy harvesters with nonlinear circuit elements (eg: AC-DC converter and/or SSHI) requires implementing equivalent circuit models in a circuit simulation software (such as SPICE) when multiple modes of vibration are taken into account. Ignoring the electromechanical back-coupling, building equivalent circuits for weakly coupled systems is simple since the equivalent circuit can be modelled only with the mechanical response being used as an input (i.e. driving voltage or current). On the other hand, Erturk and Inman showed that ignoring electromechanical back-coupling results in over estimation of generated energy for strongly coupled systems [24]. Therefore, accurate modelling of strongly coupled systems requires inclusion of electromechanical back-coupling in the equivalent circuit. Yang and Tang [51] and Elvin and Elvin [52], developed equivalent circuits including multiple-DOFs and electromechanical back-coupling. Elvin and Elvin, obtained the parameters of the equivalent circuit from Rayleigh-Ritz method while Yang and Tang used the analogy between second-order circuit equation and electromechanical coupled equation in the distributed parameter model of Erturk and Inman [19]. Elvin and Elvin [53] developed a coupled finite element analysis (FEA)-SPICE model [53] and Yang and Tang [51] extracted equivalent circuit parameters from FEA results [51] for accurate modelling of complex structures.

Although most of the above studies in the literature discussed the use of equaivalent circuit modeling for systems like cantilever beams, the implementation of this methodology is very limited for patch based harvesters attached to plate-like structures. This study presents a methodology for equivalent circuit modeling and analysis of a patch based energy harvester integrated to a thin plate using a FE model. The developed FE modeling technique is also demonstrated on a case study which involved the harvesting on a vibrating panel of a heavy duty truck cabin.

1.3. Contribution of This Thesis

The major contributions of this thesis can be summarized as follows;

- A coupled electroelastic FE model of a patch based piezoelectric energy harvester is developed and voltage and power outputs of the harvester are estimated.
- Estimated power and voltage outputs are verified with the existing distributed parameter analytical model [21].

- Equivalent circuit modeling and analysis of a patch based piezoelectric energy harvester is presented.
- System parameters of the equivalent circuit are identified from FEA by following the procedure described by Yang and Tang [51].
- Rectified voltage and power outputs of the equivalent circuit model is verified with the model developed by Shu and Lien [46].
- A real life implementation of the FE modeling methodology is demonstrated on a vibrating panel of a heavy duty truck and numerical simulations and analysis of the harvester is presented for different operating conditions of the truck.

1.4. Thesis Layout

In chapter 2, finite element modeling of the piezoceramic patch attached on an all edges clamped rectangular thin plate is presented. Frequency response functions (FRFs) relating the force input to voltage and power outputs of the energy harvester are obtained and verified with the existing analytical distributed parameter model.

In chapter 3, procedure for obtaining equivalent circuit parameters for a patch based piezoelectric energy harvester from FEA is given. Two numerical problems are studied for verification of the equivalent circuit model. In the first problem, energy harvesting circuit is simplified and included a resistive load only. Second problem includes a practical energy harvesting circuit with a full-wave bridge rectifier followed by a smoothing and a resistive load. Voltage and power FRF results of the equivalent circuit model are compared with the analytical models existing in the literature.

In chapter 4, electroelastic finite element (FE) modeling study of a patch based energy harvesting is demonstrated in a real life application. Numerical simulations of a patch-based piezoelectric energy harvester attached to a panel of a heavy duty vehicle are presented for different operating conditions.

Chapter 5, draws conclusions from the chapters and concludes the thesis with discussions of future work.

Chapter 2

FINITE ELEMENT ANALYSIS OF A PATCH BASED ENERGY HARVESTER

2.1. Overview

In this chapter, finite element analysis procedure is described for a piezoceramic patch attached on an all edges clamped rectangular thin plate. Electroelastic frequency response functions (FRFs) relating the voltage and power outputs of the energy harvester to force input are obtained and used for verification of the FE model with analytical distributed parameter model [21]. Although a practical energy circuit includes non-linear elements, such as rectifier bridge as an AC-DC converter, only a resistive load is considered here as the energy harvesting circuit. A resistive load does not fully represent a practical circuit, but it gives the information on maximum achievable power that can be extracted from the harvester. Note that the energy harvesting configuration, including a piezoceramic patch attached on a rectangular thin plate, is illustrated in Figure 1 and referred as patch based energy harvester in the rest of the chapter.

In section 2.2 FE modeling procedure is described for the patch based energy harvester. First, general information is given on piezoelectric constitutive equations, material properties and coupling type which applies to all coupled-field piezoelectric FE analysis. Then, details of modeling the patch based energy harvester is given in section 2.2.3. Brief description is given for the distributed-parameter electroelastic model of a patch based energy harvester which is later used for verification of FE modeling results. In section 2.4

voltage FRFs, peak voltage and power amplitudes and their variations with resistive load are compared for FE model and analytical model and very good agreement is observed between the results.

2.2. Finite Element Modeling

Finite element modeling of piezoelectric materials requires coupled-field analysis to take into account the interaction between structural and electrical fields. In this study, a commercial FEA package (ANSYS) is used for its coupled-field analysis capabilities for piezoelectric materials. In the following sections, first, basic information is given about the piezoelectric constitutive equations, piezoelectric material properties and coupled-field analysis. Then, coupled-field finite element (FE) analysis is implemented on a piezoelectric patch-based harvester attached to a thin plate.

2.2.1 Piezoelectric Constitutive Equations and Material Properties

Piezoelectric constitutive equations define the interaction between stress (T), strain (S), charge-density displacement (D), and electric field (E) components of piezoelectric material. Tensorial representation of the constitutive equation can be written as [54]:

$$S_{ij} = s_{ijkl}^{E} \cdot T_{kl} + d_{kij} \cdot E_k \quad (1)$$

$$D_i = d_{ikl} \cdot T_{kl} + \varepsilon_{ik}^{T} \cdot E_k \quad (2)$$

Where s_{ijkl} is elastic compliance constant, ε_{ij} is the permittivity constant and d_{ijk} is the piezoelectric constant. Superscript *E* means that compliance is measured under constant electric field and superscript *T* means that permittivity is measured under constant stress field. According to IEEE Standard on Piezoelectricity [54], 12-plane or xy-plane defines the plane of symmetry and 3-axis defines the poling direction for transversely isotropic piezoceramic materials.

Constitutive equations in equations 1 and 2 are in strain-charge form since the independent variables on the left-hand side of the equations are strain (S) and charge (D) terms. Three other forms exist for three other combinations of independent variables: stress-charge form, strain-voltage form and stress voltage form. Between these four different constitutive equations, other than strain-charge form, stress-charge form is frequently used in the literature. Stress-charge form of the constitutive equation can be written as:

$$T_{ij} = c_{ijkl}^{E} \cdot S_{kl} - e_{kij} \cdot E_k \quad (3)$$

$$D_i = e_{ikl} \cdot S_{kl} + \varepsilon_{ij}^{S} \cdot E_k \quad (4)$$

Tensorial representation of the constitutive equations is written in matrix form in equation 5.

$$\begin{bmatrix} \mathbf{S} \\ \mathbf{D} \end{bmatrix} = \begin{bmatrix} \mathbf{s}^{\mathbf{E}} & \mathbf{d}^{\mathbf{t}} \\ \mathbf{d} & \boldsymbol{\varepsilon}^{\mathbf{T}} \end{bmatrix} \begin{bmatrix} \mathbf{T} \\ \mathbf{E} \end{bmatrix} \quad (5)$$

Material property data can be converted from strain charge form to stress charge form using following equations [55].

$$\mathbf{c_E} = \mathbf{s_E}^{-1} \quad (6)$$

$$\mathbf{e} = \mathbf{d} \cdot \mathbf{s_E}^{-1} \quad (7)$$

$$\boldsymbol{\varepsilon}_\mathbf{S} = \boldsymbol{\varepsilon}_\mathbf{T} - \mathbf{d} \cdot \mathbf{s}_\mathbf{E}^{-1} \cdot \mathbf{d}^{\mathbf{t}} \quad (8)$$

Considering the piezoelectric constituve equations, one needs to define relative permittivity matrix, piezoelectric coupling matrix and elastic coefficient matrix in FEA software for a coupled-field piezoelectric analysis. In ANSYS, relative permittivity matrix can be defined with orthotropic properties including diagonal terms ε_{11}^{S}, ε_{22}^{S} and ε_{33}^{S} . It is important to note that permittivity matrix inputs are interpreted as relative permittivity unless the permittivity values are less than 1. It is possible to input relative permittivity values measured at constant stress or constant strain.

Piezoelectric matrix can be defined as piezoelectric stress matrix (i.e. e matrix is in stress charge form) or piezoelectric strain matrix form (i.e. d matrix is in strain charge form). ANSYS software converts the piezoelectric strain matrix to piezoelectric stress matrix using the relation in equation 7. Attention must be given to definition of piezoelectric stress matrix. While ANSYS uses standard structural mechanics format, piezoelectric material properties are mostly defined in IEEE Standard notation. In IEEE format row order is $\{x, y, z, yz, xz, xy\}$ while it is $\{x, y, z, xy, yz, xz\}$ in ANSYS. Therefore piezoelectric matrix must be converted from IEEE format to ANSYS format as shown in equation9.

$$\mathbf{d}_{\mathbf{IEEE}}^{\mathbf{T}} = \begin{bmatrix} d_{11} & d_{21} & d_{31} \\ d_{21} & d_{22} & d_{23} \\ d_{31} & d_{32} & d_{33} \\ d_{41} & d_{42} & d_{43} \\ d_{51} & d_{52} & d_{53} \\ d_{61} & d_{62} & d_{63} \end{bmatrix} \quad \mathbf{d}_{\mathbf{ANSYS}}^{\mathbf{T}} = \begin{bmatrix} d_{11} & d_{21} & d_{31} \\ d_{21} & d_{22} & d_{23} \\ d_{31} & d_{32} & d_{33} \\ d_{61} & d_{62} & d_{63} \\ d_{51} & d_{52} & d_{53} \\ d_{41} & d_{42} & d_{43} \end{bmatrix} \quad (9)$$

Elastic coefficients matrix can include either stiffness or compliance coefficients. Similar to piezoelectric matrix, order of rows of the elastic coefficients matrix must be converted from IEEE format to ANSYS format.

$$\mathbf{c}^{\mathbf{E}}_{\mathbf{IEEE}} = \begin{bmatrix} c_{11} & & & & & \\ c_{21} & c_{22} & & & & \\ c_{31} & c_{31} & c_{33} & & & \\ c_{41} & c_{42} & c_{43} & c_{44} & & \\ c_{51} & c_{52} & c_{53} & c_{54} & c_{55} & \\ c_{61} & c_{62} & c_{63} & c_{64} & c_{65} & c_{66} \end{bmatrix} \quad \mathbf{c}^{\mathbf{E}}_{\mathbf{ANSYS}} = \begin{bmatrix} c_{11} & & & & & \\ c_{21} & c_{22} & & & & \\ c_{31} & c_{31} & c_{33} & & & \\ c_{61} & c_{62} & c_{63} & c_{66} & & \\ c_{51} & c_{52} & c_{53} & c_{54} & c_{55} & \\ c_{41} & c_{42} & c_{43} & c_{44} & c_{45} & c_{46} \end{bmatrix} \quad (10)$$

2.2.2 Coupling Method and Element Description

In coupled-field problems, two different coupling methods exist including direct coupling and sequential (load transfer) methods. Both methods are available in ANSYS for coupled-field analysis [56]. Direct coupling method uses coupled-field elements including all degrees of freedoms of multiple fields. Coupled-field element allows assembly and solution of a single matrix system of equations (including all degrees of freedoms of included fields) in single analysis. In load transfer method, separate analyses must be performed for each physical field. The fields are coupled by transferring results of one field equations to another set of field equations until a final solution is obtained.

If the coupled-field analyses include weakly coupled fields or the interactions between physics are not non-linear, load transfer method is more advantageous than coupled field method considering the processing power and memory cost of coupled-field analyses. In case of strong coupling between two physical fields, such as piezoelectric analysis, direct coupling method is used for its capability of obtaining results in single analysis by making use of coupled-field elements to solve the interactions between fields directly.

In this study, direct coupling of the structural and electrical fields of piezoelectric materials is achieved by 3D, 20-node coupled field SOLID 226 element of ANSYS as shown in Figure 2.

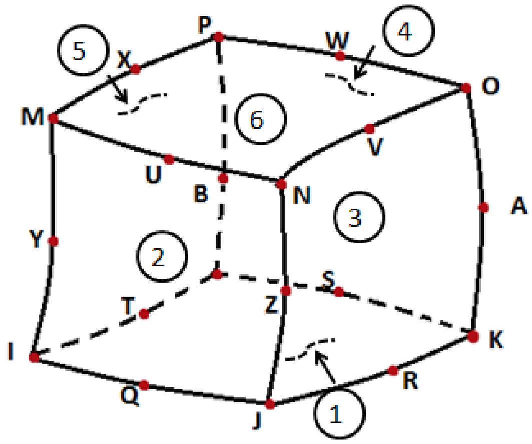

Figure 2. Geometry of 3D, 20-node coupled field SOLID 226 element, reproduced from ANSYS Element Reference[56]

For the piezoelectric analysis, the coupled-field element has 4 DOFs for each node including translation in x, y and z directions and voltage. Reaction solutions include force and electric charge values. The element is available for static, modal, full harmonic and full transient analysis. The matrix equation for direct coupling with coupled field element is given in equation 11.

$$\begin{bmatrix} [M] & 0 \\ 0 & 0 \end{bmatrix} \begin{Bmatrix} \{\ddot{u}\} \\ \{\ddot{V}\} \end{Bmatrix} + \begin{bmatrix} [C^u] & 0 \\ 0 & [C^v] \end{bmatrix} \begin{Bmatrix} \{\dot{u}\} \\ \{\dot{V}\} \end{Bmatrix} + \begin{bmatrix} [K^u] & [K^Z] \\ [K^Z]^T & [K^V] \end{bmatrix} \begin{Bmatrix} \{u\} \\ \{V\} \end{Bmatrix} = \begin{Bmatrix} \{F\} \\ \{L\} \end{Bmatrix} \quad (11)$$

Structural terms in equation 11 are mass matrix M, damping matrix C^u, stiffness matrix K^u, nodal displacement vector u, and nodal force vector F. Dielectric terms are damping permittivity matrix C^v, electric potential vector V and electric charge vector L. Strong coupling is achieved by off diagonal stiffness submatrices K^Z.

ANSYS also provides piezoelectric circuit elements (CIRCU94) to be used for coupled piezoelectric-circuit analysis. Circuit elements can be used to model resistor, inductor, capacitor, independent current source and independent voltage source. It is important to note that piezoelectric circuit elements cannot be used for modeling non-linear components such as diodes. Therefore, a realistic non-linear energy harvesting circuit cannot be connected to a piezoelectric FE model as discussed in section 2.1. However, the energy harvesting circuit can be represented by a resistive load directly attached to the piezoelectric FE model and maximum achievable power output of the piezoelectric energy harvester can be obtained.

2.2.3 Modeling Patch-Based Energy Harvester

In this section, FE modeling procedure is described for a patch based energy harvester, as illustrated in Figure 3. Following the common approach in literature, the energy harvesting circuit is represented by a single resistive load connected to the top and bottom electrodes of the piezoceramic patch and full conductivity of the electrodes are taken into account. Focus is given to the voltage and power outputs measured on the resistive load due to point excitation force acting on the host structure.

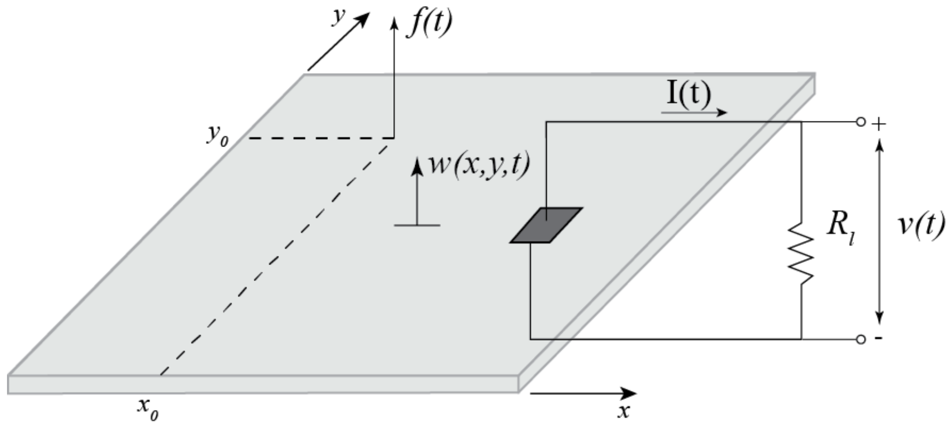

Figure 3. Piezoceramic patch attached on the thin rectangular host structure.

. The finite element model of the described structure is shown in Figure 4. Note that Figure **4** is a coarse display model given for illustration only and does not show the original number of elements used in the analysis. The host plate is meshed with 20-node structural solid elements (SOLID186) and the piezoceramic patch is meshed with 20-node coupled-field solid elements (SOLID226) which is explained in detail in section 2.2.2. All degrees of freedoms (DOF) of the ends of the host plate are constrained to be zero. The piezoceramic patch and the host structure are tied together via CEINTF command in ANSYS, which generates constraint equations relating the nodes at the bonding interfaces. Therefore, bonding between the host structure and the piezoceramic patch is assumed to be perfect.

To simulate the highly conductive top and bottom electrode layers of the harvester patch, the voltage degrees of freedoms (DOFs) on bottom and top surfaces are forced to be equipotential by creating a coupled DOF set for each surface. CIRCU94 piezoelectric circuit element is used for simulating the resistive load connected to the piezoceramic patch. One end of the piezoelectric circuit element is connected to the top electrode and the other end is connected to the grounded bottom electrode to include two-way electromechanical coupling and measure the voltage output.

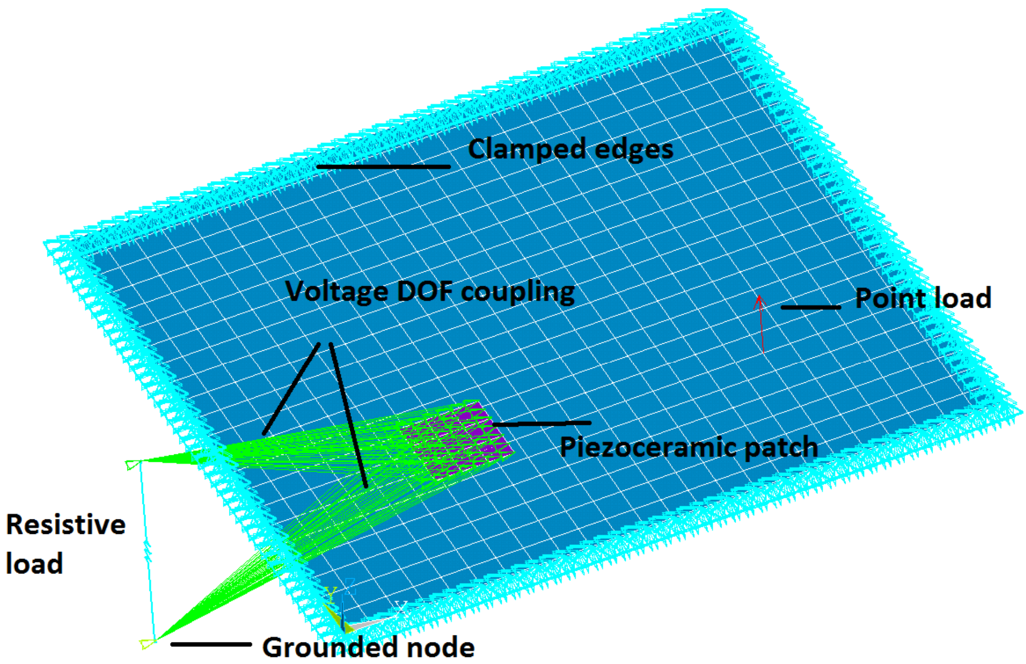

Figure 4. Finite element model of patch based energy harvester.

2.3. Distributed Parameter Analytical Model

In this section, a brief description is given for the distributed-parameter electroelastic model of a thin plate with a piezoceramic patch harvester which is introduced by Aridogan et al. based on Kirchhoff's plate theory for all four edges clamped (CCCC) boundary conditions [21]. The host plate and the structurally integrated piezoceramic patch harvester are shown in Figure 5.

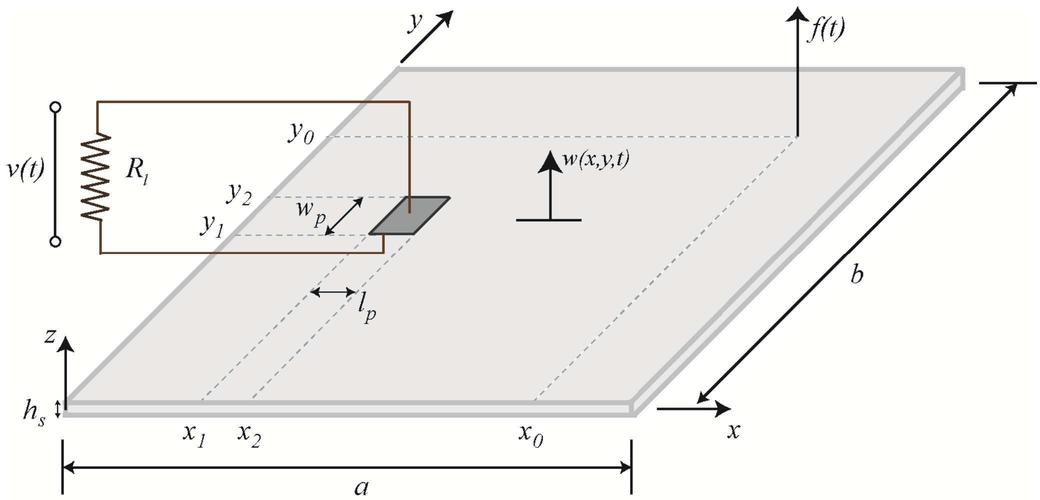

Figure 5. Piezoceramic patch attached on a thin rectangular plate for patch based energy harvesting [21].

Transverse point force $f(t)$ is acting at the position (x_0, y_0). l_p and w_p are the length and width of the piezoceramic patch respectively. Corners of the piezoceramic patch covers a rectangular region with two corners at (x_1, y_1) and (x_2, y_2). The length and width of the host plate are a and b, respectively. Thicknesses of the host plate is h_s and thickness of the piezoceramic patch is h_p. Again the energy harvesting circuit is represented by a resistive load (R_l) which is connected to the perfectly conductive top and bottom electrodes with negligible thickness. Piezoceramic patch is assumed to be coupled to the host only electromechanically with negligible mass and stiffness contribution.

The differential equation governing the mechanical motion of the host plate and the piezoceramic patch with electrical coupling can be written as

$$
\begin{aligned}
& D\left(\frac{\partial^4 w(x,y,t)}{\partial x^4}+2\frac{\partial^4 w(x,y,t)}{\partial x^2\partial y^2}+\frac{\partial^4 w(x,y,t)}{\partial y^4}\right)+c\frac{\partial w(x,y,t)}{\partial t}+\rho_s h_s\frac{\partial^2 w(x,y,t)}{\partial t^2} \\
& -\theta v(t)\left\{\left[\frac{\mathrm{d}\delta(x-x_1)}{\mathrm{d}x}-\frac{\mathrm{d}\delta(x-x_2)}{\mathrm{d}x}\right]\left[H(y-y_1)-H(y-y_2)\right]\right. \\
& \left.+\left[\frac{\mathrm{d}\delta(y-y_1)}{\mathrm{d}y}-\frac{\mathrm{d}\delta(y-y_2)}{\mathrm{d}y}\right]\left[H(x-x_1)-H(x-x_2)\right]\right\} \\
& = f(t)\delta(x-x_0)\delta(y-y_0)
\end{aligned} \qquad (12)
$$

where $w(x,y,t)$ is transverse deflection of the plate at position (x,y) and at time t. The mass density of the plate is ρ_s and c is the external damping parameter (viscous air damping). The Dirac delta functions are $\delta(x)$ and $\delta(y)$ along the x and y directions. The bending stiffness of the plate is $D = Y_s h_s^3/(12-12\nu_s{}^2)$, while its Young's modulus and Poisson's ratio are Y_s and ν_s. $H(x)$ and $H(y)$ are the Heaviside functions and $v(t)$ is the voltage across the external resistive load. The electromechanical term θ is defined as $\theta = \bar{e}_{31} h_{pc}$, which is the multiplication of effective piezoelectric constant $\bar{e}_{31}$ and reference distance h_{pc} of the center layer of the piezoceramic patch to the reference surface at the location of the patch.

The governing equation of the coupled circuit dynamics can be expressed as

$$
C_p\frac{\mathrm{d}v(t)}{\mathrm{d}t}+\frac{v(t)}{R_l}+\theta\left\{\int_{y=y_1}^{y_2}\int_{x=x_1}^{x_2}\left[\frac{\partial^3 w(x,y,t)}{\partial x^2\partial t}+\frac{\partial^3 w(x,y,t)}{\partial y^2\partial t}\right]\mathrm{d}x\ \mathrm{d}y\right\}=0 \quad (13)
$$

where C_p is the capacitance of the piezoceramic patch and defined as $C_p = \left(\bar{\varepsilon}_{33}^{S} w_p l_p\right) / h_p$.

By conducting the modal analysis procedure for a two-dimensional structure, electromechanically coupled ordinary differential equations of the plate in modal coordinates can be written as:

$$\frac{\mathrm{d}^2\eta_{mn}(t)}{\mathrm{d}t^2} + 2\zeta_{mn}\omega_{mn}\frac{\mathrm{d}\eta_{mn}(t)}{\mathrm{d}t} + \omega_{mn}^2\eta_{mn}(t) - \tilde{\theta}_{mn}v(t) = f_{mn}(t) \tag{14}$$

$$C_p\frac{\mathrm{d}v(t)}{\mathrm{d}t} + \frac{v(t)}{R_l} + \sum_{n=1}^{\infty}\sum_{m=1}^{\infty}\tilde{\theta}_{mn}\frac{\mathrm{d}\eta_{mn}(t)}{\mathrm{d}t} = 0 \tag{15}$$

Here, ω_{mn} is the undamped natural frequency for the mn-th vibration mode and ζ_{mn} is the damping ratio. The modal forcing in equation (14) is

$$f_{mn} = \int_0^b \int_0^a f(t)\delta(x - x_0)\delta(y - y_0)\phi_{mn}(x, y)\,\mathrm{d}x\,\mathrm{d}y = f(t)\phi_{mn}(x_0, y_0) \tag{16}$$

while the electromechanical coupling term $\tilde{\theta}_{mn}$ can be given by

$$\tilde{\theta}_{mn} = \theta\left[\int_{y_1}^{y_2}\left.\frac{\partial\phi_{mn}(x, y)}{\partial x}\right|_{x_1}^{x_2}\mathrm{d}y + \int_{x_1}^{x_2}\left.\frac{\partial\phi_{mn}(x, y)}{\partial y}\right|_{y_1}^{y_2}\mathrm{d}x\right] \tag{17}$$

Assuming a harmonic force excitation $f(t) = F_0 e^{j\omega t}$, where the amplitude of the force is F_0 and ω is the excitation frequency, the steady-state voltage response $v(t)$ across the resistive load is obtained as

$$v(t) = Ve^{j\omega t} = \frac{-j\omega \sum_{n=1}^{\infty} \sum_{m=1}^{\infty} \frac{F_0 \phi_{mn}(x_0, y_0)\, \tilde{\theta}_{mn}}{\omega_{mn}^2 - \omega^2 + j2\zeta_{mn}\omega_{mn}\omega}}{j\omega C_p + \frac{1}{R_l} + \sum_{n=1}^{\infty} \sum_{m=1}^{\infty} \frac{j\omega \tilde{\theta}_{mn}^2}{\omega_{mn}^2 - \omega^2 + j2\zeta_{mn}\omega_{mn}\omega}} e^{j\omega t} \quad (18)$$

2.4. Verification of the FE Model Results with Analytical Model

Having described FE and the distributed parameter analytical modeling procedure for a patch based energy harvester, in this section, power and voltage output results of the FE model are compared using a numerical example. Geometry and FE model of the problem is illustrated in Figure 3 and Figure 4, respectively. Geometric and material properties of the numerical example are listed in Table 1.

Table 1. Geometric, material and electroelastic properties

Property	Aluminum	Piezoceramic
Length (mm)	580	72.4
Width (mm)	540	72.4
Thickness (mm)	1.96	0.267
Young’s modulus (GPa)	70	69
Mass density (kg/m^3)	2700	7800
Piezoelectric constant e_{31}(C/m^2)	-	-190
Permittivity constant $\bar{\varepsilon}_{33}^S$ (nF/m)	-	9.57
Damping ratio ζ_{mn}	0.01	0.01

Transverse point force is applied at $x_0 = 470\,mm,\ y_0 = 150\,mm$ location. As discussed in Section 2.2.3, electrodes of the piezoceramic patch are assumed to be perfectly conductive. The piezoelectric energy harvesting circuit is represented only by a resistive element due to limitations of both FE model and distributed parameter analytical model.

With given geometry, constraints and loads for the FE model, a convergence test is conducted to confirm that element discretization is fine enough to get accurate results. Initially, only the host structure is taken into account for the test and piezoceramic patch is ignored. At each step of the convergence test, numbers of elements along the edges of the host structure are increased, while the number of elements through the thickness is fixed to one. The first natural frequencies, ω_{11}, are recorded for each step and relative errors between consecutive steps are calculated. Figure 6 shows the variation of relative error with increasing number of elements along the edges. After 18 elements, relative error becomes lower than 1% and using 54 elements results in 0.11% relative error. Limiting the relative error to maximum 0.2%, 54 or higher number of elements can be used along the edges. Next, numbers of elements along the edges are fixed to 54 and number of elements through the thickness of the host structure is increased. For this case, relative error is not only calculated for the first natural frequency, but also for harmonic response at corner location, (x_1,y_1), of the piezoceramic patch due to harmonic transverse point force acting at 60Hz.

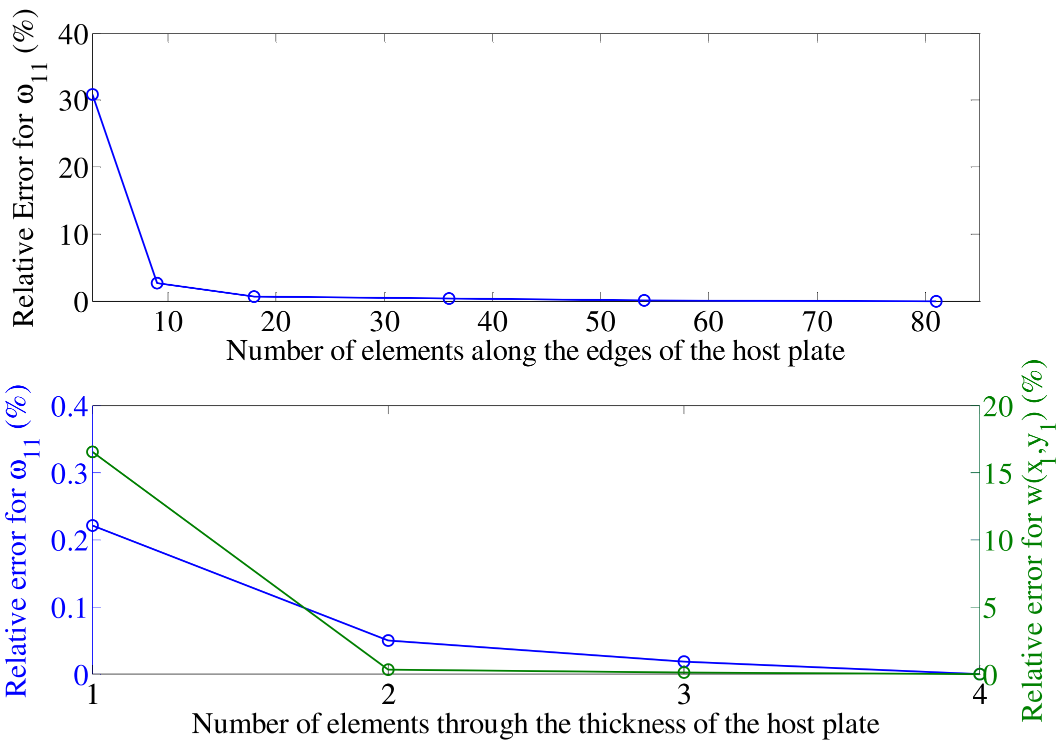

Figure 6. Variation of relative error with number of elements along the edges and through the thickness of the host plate.

Figure 6 shows that, for the first natural frequency, two elements through the thickness results in relative error lower than 0.2%, while the relative error for displacement is lower than 0.2% only after three elements are used through the thickness. Therefore, for the host plate, minimum three elements are required through the thickness. Now the number of elements for the host plate is determined and piezoceramic patch can be included in the convergence test. Considering negligible mass of the piezoceramic patch compared to host structure, convergence test is only conducted for voltage response measured on the resistive circuit element due to harmonic transverse point load. The procedure is similar to the one used for the host plate. First, number of elements through the thickness is fixed and numbers of elements along the edges are increased. Figure 7 shows that, after 15 elements along the edges, relative error becomes less than 0.2%. Then, numbers of elements along edges are fixed to 15 and number of elements along the thickness is increased. For the voltage response of the piezoceramic patch, one element through the thickness results in 0.05% relative error. Therefore, for the piezoceramic patch, using 15 elements along the edges and single element along the thickness is convenient for this verification study.

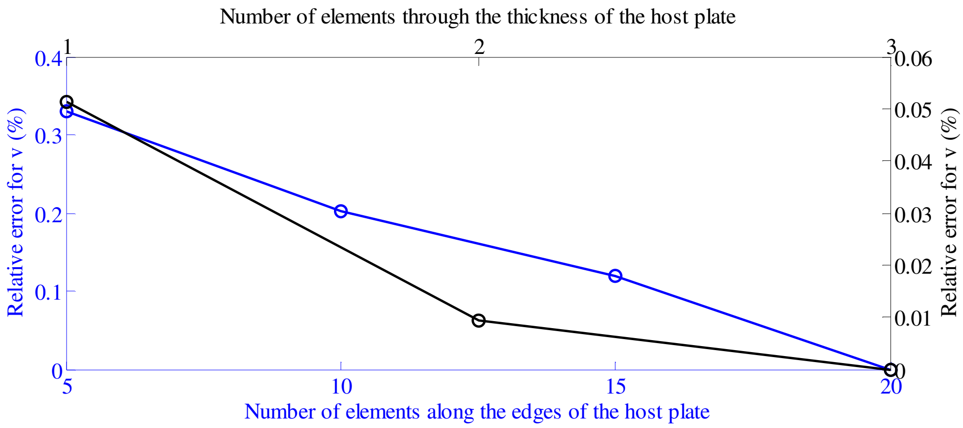

Figure 7. Variation of relative error with number of elements along the edges and through the thickness of the piezoceramic patch.

After required number of elements are determined for the FE model, electroelastic frequency response functions (FRFs) relating the voltage and power outputs of the energy harvester to force input are obtained and used for comparison of the FE model and the distributed parameter model results. To obtain the frequency response functions in ANSYS, harmonic analysis is performed with unit input force and voltage difference is measured at the nodes of the resistive circuit element. Analytical model results are obtained by using the closed-form relation in Equation 18. Voltage FRF of the harvester under the effect of the harmonic force is shown in Figure 8 for various resistive load cases (ranging from 100 Ω to 1 MΩ).

In Figure 8, it is observed that voltage amplitudes from FE model are in good agreement with those obtained from the analytical model with a slight shift in natural frequencies. Comparison of short circuit natural frequencies is given for the first four modes in Table 2.

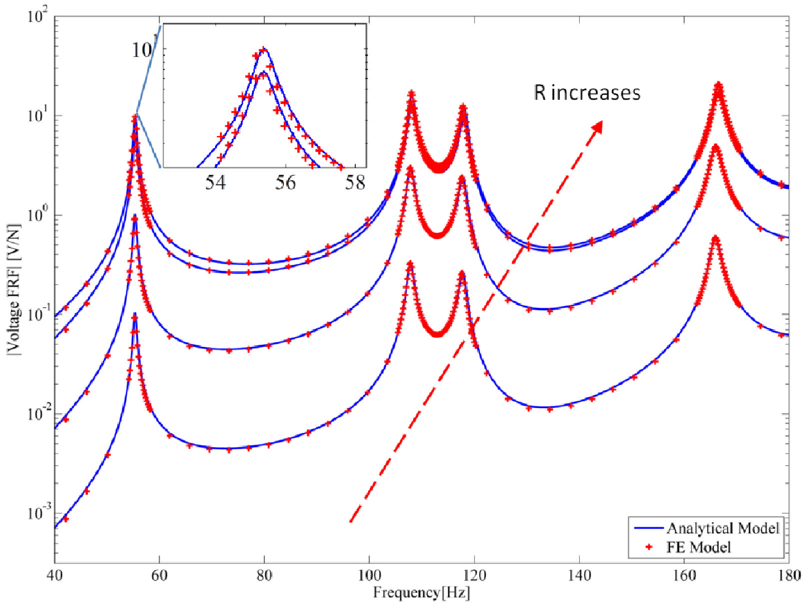

Figure 8. Voltage FRF comparison of FE model and analytical model results.

Table 2. Comparison of short circuit natural frequencies for FE model and analytical model.

Resonance Frequencies (Hz)	FE Model	Analytical
ω_{11}^{sc}	55.08	55.34
ω_{21}^{sc}	107.35	107.82
ω_{12}^{sc}	117.20	117.83
ω_{22}^{sc}	165.30	165.93

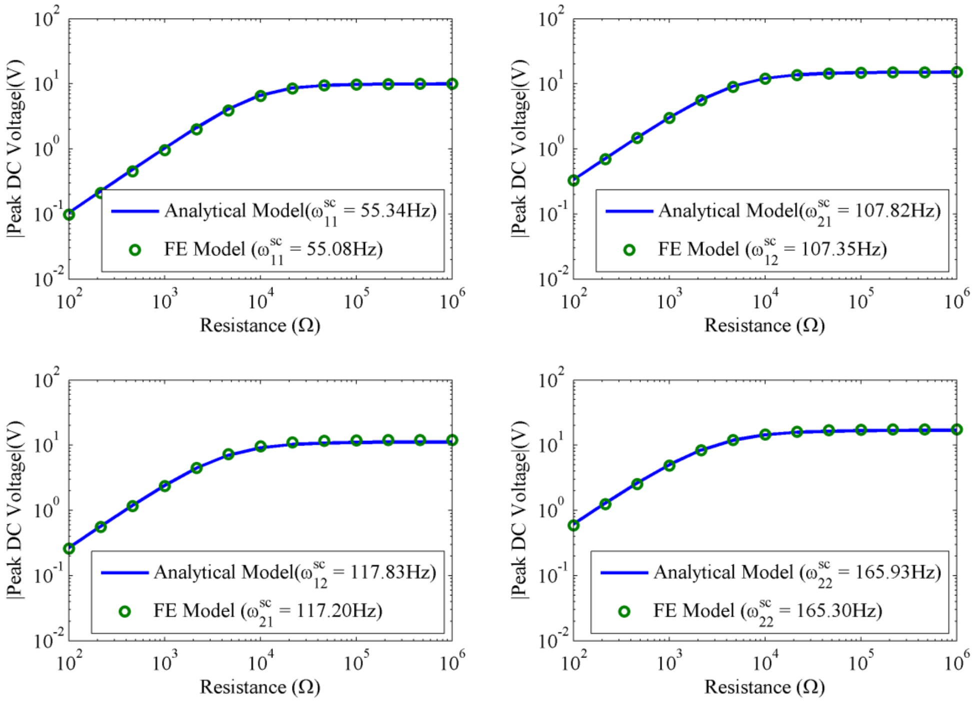

Figure 9. Voltage outputs for a wide range of resistive loads at first four short circuit natural frequencies

Figure 9 presents the voltage amplitudes at first four short circuit natural frequencies for the analytical model and the FE model. It can be observed from the figure that the FE model accurately predicts the natural frequencies and peak voltage amplitudes. It is also observed that peak voltage amplitudes increase with increasing resistive load and remains constant after open circuit condition is achieved (i.e. resistive load $R_l \to \infty$).

Having determined variation of peak voltage amplitudes with changing resistive load, one can obtain the variation of power outputs as presented in Figure 10 simply by using the power equation, $P = \frac{V^2}{R}$. Variation of power output is similar for each vibration mode. Power output reaches to its maximum for the optimum resistance value.

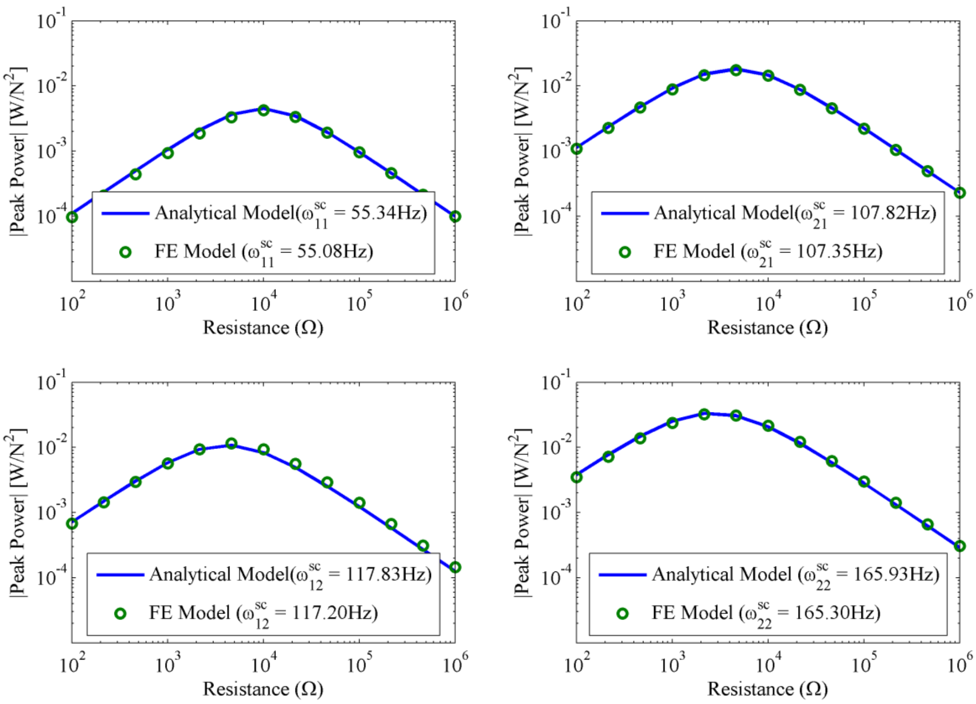

Figure 10. Power outputs for a wide range of resistive loads at first four short circuit natural frequencies

Chapter 3

EQUIVALENT CIRCUIT MODELLING OF A PATCH BASED ENERGY HARVESTER

3.1. Overview

In modeling of piezoelectric energy harvesters, usually a simple resistive load is used to estimate power outputs. However, practical energy harvesters require more complex interface circuits to provide a stable DC signal for storage devices. Simplest practical circuit includes a rectifier bridge as an AC-DC converter followed by a smoothing capacitor. Analytical solutions of piezoelectric energy harvesters with practical circuits are also limited with simplified mechanical conditions. Therefore simulation of piezoelectric energy harvesters with nonlinear circuit elements (eg: AC-DC converter and/or SSHI) requires implementing equivalent circuit models in a circuit simulation software (such as SPICE) when both complex mechanical conditions and practical circuits are taken into account.

In this chapter, first, equivalent circuit representation of piezoelectric transducers are presented in Section 3.2. The procedure for obtaining equivalent circuit parameters for a patch based energy harvester is presented in Section 3.2.1. In Section 3.3, two numerical validation problems are studied. First problem is focused on the simplified resistive energy harvesting circuit in order to compare the results with the distributed parameter analytical model. Second example takes into account a practical energy harvesting circuit including a full-wave bridge rectifier and a smoothing capacitor. Since the distributed parameter analytical model can not model non-linear circuit elements in the energy harvesting circuit and non linear circuit elements are not compatible with piezoelectric elements in ANSYS, a lumped parameter analytical model is used for validation of the second problem.

3.2. Equivalent Circuit Representation

Equivalent circuit representation of piezoelectric energy harvesters is based on the analogy between mechanical domain and electrical domain relations. For example, relation between force and velocity for a rigid mass is mathematically analogous to constitutive equation of an electric inductor as shown in equations 19 and 20 [57].

$$F = m\frac{d^2x}{dt^2} \quad (19) \qquad\qquad v = L\frac{d^2q}{dt^2} \quad (20)$$

Analogy between equations 19 and 20 implies that the role of force F , velocity u and mass m in mechanical domain corresponds to voltage v , charge i and inductance L in electrical domain respectively. This type of analogy is defined as direct-analogy resulting in a correspondence between through variable (force and current) in one domain and across variable (voltage and velocity) in the other domain. Direct analogy between mechanical and electrical quantities is summarized in Table 3.

Table 3. Summary of direct analogy between mechanical and electrical quantities

Mechanical Parameters	Electrical Parameters
Force	Voltage
Velocity	Current
Displacement	Charge
Momentum	Magnetic flux linkage
Mass	Inductance
Compliance	Capacitance
Viscous Resistance	Resistance

Governing equations of the patch based energy harvester are derived in Section 2.3 and given once again in equations 21 and 22.

$$\frac{\mathrm{d}^2\eta_{mn}(t)}{\mathrm{d}t^2} + 2\zeta_{mn}\omega_{mn}\frac{\mathrm{d}\eta_{mn}(t)}{\mathrm{d}t} + \omega_{mn}^2\eta_{mn}(t) - \tilde{\theta}_{mn}v(t) = f_{mn}(t) \quad (21)$$

$$C_p\frac{\mathrm{d}v(t)}{\mathrm{d}t} + \frac{v(t)}{R_l} + \sum_{n=1}^{\infty}\sum_{m=1}^{\infty}\tilde{\theta}_{mn}\frac{\mathrm{d}\eta_{mn}(t)}{\mathrm{d}t} = 0 \quad (22)$$

Equation 21 is the governing equation for the modal mechanical coordinates including the mechanical quantities and equation 22 represents the governing electrical circuit equation with electrical quantities. Equations are coupled with the modal electromechanical coupling term $\tilde{\theta}_{mn}$. Utilizing the direct analogy between mechanical quantities in equation 22 and electrical quantities in equation 23, electrical and mechanical components of the energy harvester can be modeled separately as equivalent circuits with electromechanical coupling defined as a transformer between mechanical and electrical sides. Equivalent circuit parameters and their mechanical counterparts for the distributed parameter model are given in

Table 4.

Table 4. Analogy between electrical and mechanical domains of piezoelectric patch-based harvester

Equivalent circuit parameters at mn-th mode	Mechanical counterparts
Voltage source: $V_{mn}(t)$	Modal point force: $f_{mn}(t)$
Inductance: $L_{mn}(t)$	1
Resistance: $R_{mn}(t)$	$2\zeta_{mn} w_{mn}$
Capacitance: $C_{mn}(t)$	$1/w_{mn}$
Ideal Transformer ratio: N_{mn}	$-\tilde{\theta}_{mn}$
Electrical charge: $q_{mn}(t)$	Modal time response: $\eta_{mn}(t)$
Electrical current: $i_{mn}(t)$	$d\eta_{mn}(t)/dt$

Once the parameters of the equivalent circuit model are obtained from the analytical model by using the analogy in

Table 4, equivalent circuit model can be built as shown in Figure 11. The equivalent circuit makes use of decoupled equations in modal coordinate space and can be extended to include any number of mechanical modes. Furthermore, using the equivalent circuit representation, any practical circuit can be included in the electrical part of the circuit.

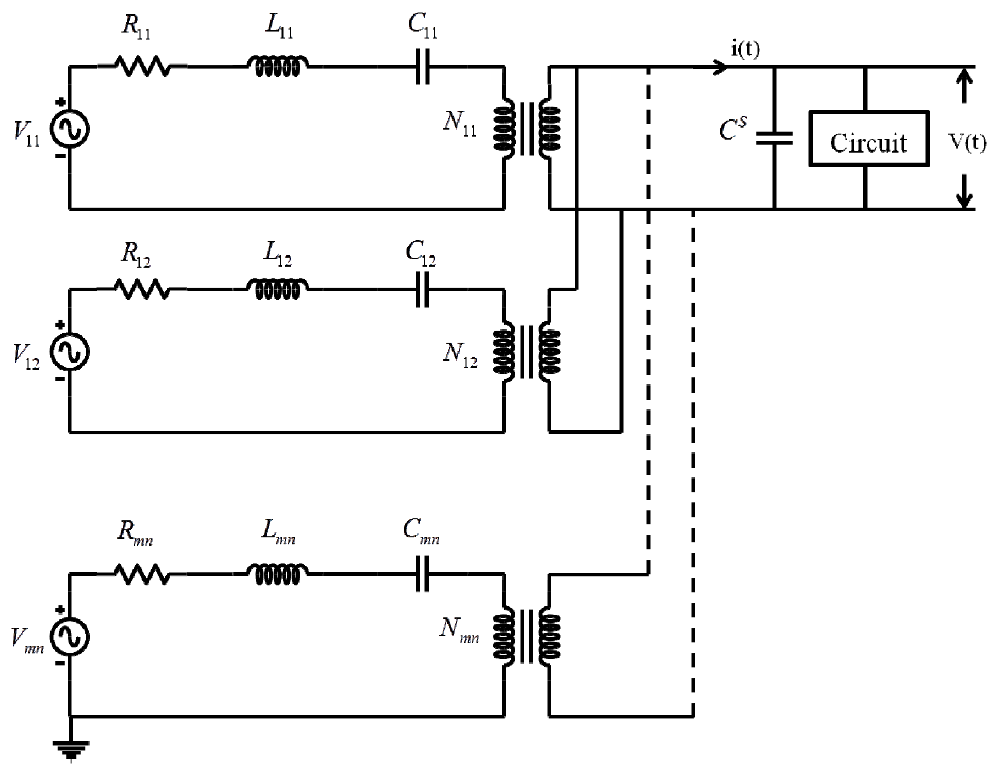

Figure 11. Equivalent circuit model representation of the patch based energy harvester.

Another configuration of the circuit can be obtained by converting the elements on the left side of the ideal transformer to right side of the transformer using the relations in equation 23. Alternative configuration of the circuit is given in Figure 12.

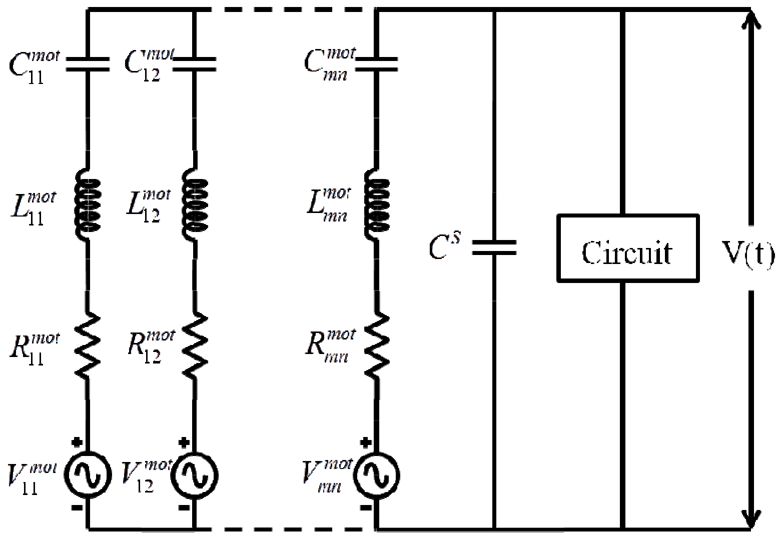

Figure 12. Equivalent circuit without ideal transformer with converted circuit parameters

$$L_{mn}^{mot} = \frac{L_{mn}}{N_{mn}^{\ 2}} \quad R_{mn}^{mot} = \frac{R_{mn}}{N_{mn}^{\ 2}} \quad C_{mn}^{mot} = C_{mn} N_{mn}^{\ 2} \quad v_{mn}^{mot} = \frac{v_{mn}}{N_{mn}} \quad (23)$$

If an analytical solution does not exist for the problem, then the analogy in

Table 4 cannot be directly applied to obtain the equivalent circuit parameters. In this case, it is possible to identify the equivalent circuit parameters by FE analysis of the harvester following the procedure presented by Yang and Tang [51]. Procedure for identification of equivalent circuit parameters from the FE model can be summarized as follows:

- Determine static clamped capacitance with static FE analysis or analytically using the relation $C^S = \varepsilon_{33}^S A_p / h_p$ where A_p is the area and h_p is the thickness of the piezoceramic patch.

- Perform modal analysis and determine short circuit resonance frequency of each vibration mode.
- Perform harmonic analysis with alternating voltage input and obtain admittance to identify passive circuit parameters C_{mn}, L_{mn}, R_{mn}, N_{mn} for each mode.
- Perform finite element harmonic analysis, with force applied, to obtain the charge response. Determine v_{mn} using charge response.

3.2.1 Identification of Equivalent Circuit Parameters by FE Analysis

Passive equivalent circuit parameters $C_{mn}, L_{mn}, R_{mn}, N_{mn}$ can be obtained from total admittance of the piezoelectric energy harvester. Harmonic voltage input is applied to the piezoceramic patch in the FE model and total admittance is obtained simply by division of current response to voltage input ($Y = j\omega Q / V$). Total admittance can be expressed as summation of damped admittance Y_d and motional admittance Y_{mot} [51].

$$Y = j\omega\left(C_{mn}^{d} + \frac{C_{mn}^{mot}}{1 - L_{mn}^{mot} C_{mn}^{mot} \omega^2 + jR_{mn}^{mot} C_{mn}^{mot} \omega} \right)$$

$$Y = Y_d + Y_{mot} \quad (24)$$

Damped admittance and motional admittance are given as follows from equation 24:

$$Y_d = j\omega C_{mn}^{d} \quad (25)$$

$$Y_{mot} = \frac{j\omega C_{mn}^{mot}}{1 - L_{mn}^{mot} C_{mn}^{mot} \omega^2 + jR_{mn}^{mot} C_{mn}^{mot} \omega} \quad (26)$$

Y_{mot} can be directly obtained from FE analysis results by excluding Y_d from the calculated total admittance for each mode. Y_d is simply the imaginary part of the total admittance at each natural frequency [51]:

$$Y_d = \mathrm{Im}[Y(\omega_{mn})] \quad (27)$$

Having determined Y_{mot} for each vibration mode, equivalent circuit parameters C_{mn}^{mot}, L_{mn}^{mot}, R_{mn}^{mot} and N_{mn} can be determined from the admittance locus using following relations:

$$\begin{aligned} R_{mn}^{mot} &= \frac{1}{\max[\mathrm{Re}(Y_{mot})]} \\ L_{mn}^{mot} &= \frac{R_{mn}^{mot}}{\omega[\min[\mathrm{Im}(Y_{mot})]] - \omega[\max[\mathrm{Im}(Y_{mot})]]} \\ C_{mn}^{mot} &= \frac{1}{\omega_{mn}{}^{2} L_{mn}^{mot}} \\ N_{mn} &= \sqrt{\frac{1}{L_{mn}^{mot}}} \end{aligned} \quad (28)$$

With parameters C_{mn}, L_{mn}, R_{mn} and N_{mn}, now equivalent voltage source v_{mn} can be determined. With unit harmonic force applied, charge response can be obtained from FE analysis. With determined R_{mn} and N_{mn} equivalent voltage source can be determined using equation 29 [51].

$$v_{mn} = N_{mn} R_{mn}^{mot} j\omega_{mn} Q(j\omega_{mn}) \quad (29)$$

3.3. Validation of the Equivalent Circuit Model

In this section, equivalent circuit model of the patch based piezoelectric energy harvester is constructed in SPICE software and simulation results are validated for two different validation examples with different circuit configurations. The first configuration includes a resistive load only as a simplified harvesting circuit with AC output. This configuration is referred as AC Problem in this chapter and illustrated in Figure 13(a). Equivalent circuit model results for AC configuration are compared with the FE analysis results presented in Chapter 2.

Second circuit configuration includes a practical energy harvesting circuit with a full-wave bridge rectifier followed by a smoothing capacitor as shown in Figure 13(b). This problem is referred as DC problem and voltage and power output results of the DC problem are compared with lumped parameter model suggested by Shu and Lien [46].

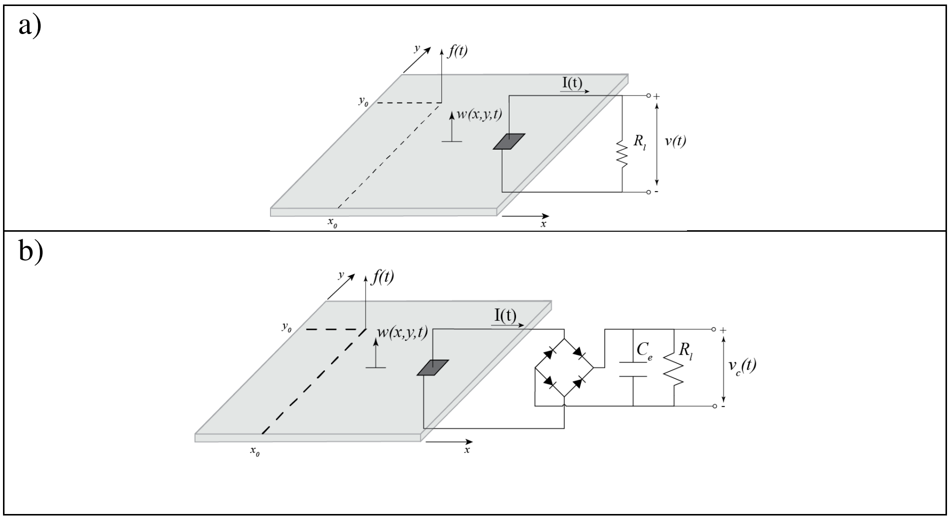

Figure 13. (a) Piezoceramic patch connected to resistive load in AC problem, (b) Piezoceramic patch connected to practical energy harvester circuit in DC problem

Geometric and material properties of the patch based harvester and the host structure are the same for both problems and given in Table 5. Transverse point force is applied at

$x_0 = 650mm,\ \ y_0 = 50mm$ location. As discussed in Section 2.2.3, electrodes of the piezoceramic patch are assumed to be perfectly conductive.

Table 5 Geometric, material and electroelastic properties

Property	Aluminum	Piezoceramic
Length (mm)	580	72.4
Width (mm)	540	72.4
Thickness (mm)	1.96	0.267
Young's modulus (GPa)	70	69
Mass density (kg/m^3)	2700	7800
Piezoelectric constant e_{31}(C/m^2)	-	-190
Permittivity constant $\bar{\varepsilon}_{33}^{S}$ (nF/m)	-	9.57
Damping ratio ζ_{mn}	0.01	0.01

3.3.2 AC Problem Validation

In the AC problem, energy harvesting circuit is represented by a resistor attached to the piezoceramic patch as shown in Figure 13(a).

Total admittance of the harvester is directly obtained from the FE model, for each mode, by performing harmonic analysis with alternating voltage input applied between top and bottom electrodes of the piezoceramic patch. Motional admittance is then obtained by extracting damped admittance component from total admittance using equation 27. Motional admittance locus plots, showing real and imaginary parts of the motional admittance, are given in Figure 14 for the first five modes.

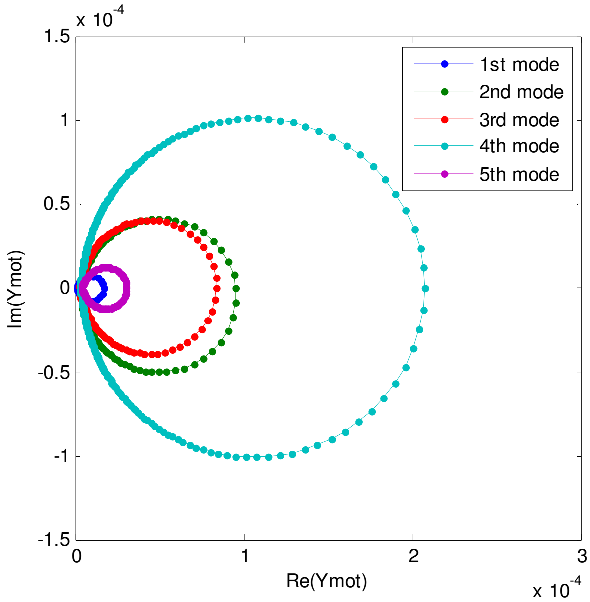

Figure 14. Motional admittance locus of the first five modes.

Passive equivalent circuit parameters of the multi-mode equivalent circuit model are identified from motional admittance locus plots using relations in equation 28 as described in Section 3.2.1. Additionally, unit harmonic force is applied to the host structure in the FE model and charge response is obtained to be further used to identify equivalent voltage source using equation 29. Having determined equivalent circuit parameters, equivalent circuit can be built in SPICE.

Performing AC sweep analysis in SPICE software, voltage FRF of the patch based energy harvester is obtained for various resistive load cases (ranging from 100 Ω to 1 MΩ). Good agreement is observed between FE model and equivalent circuit model in Figure 15. Only at low frequencies, voltage amplitudes are higher for equivalent circuit model results. That is due to the difference in number of modes included in the FE model and equivalent circuit model. While FE model uses full method in the solution, equivalent model includes superposition of first nine modes only.

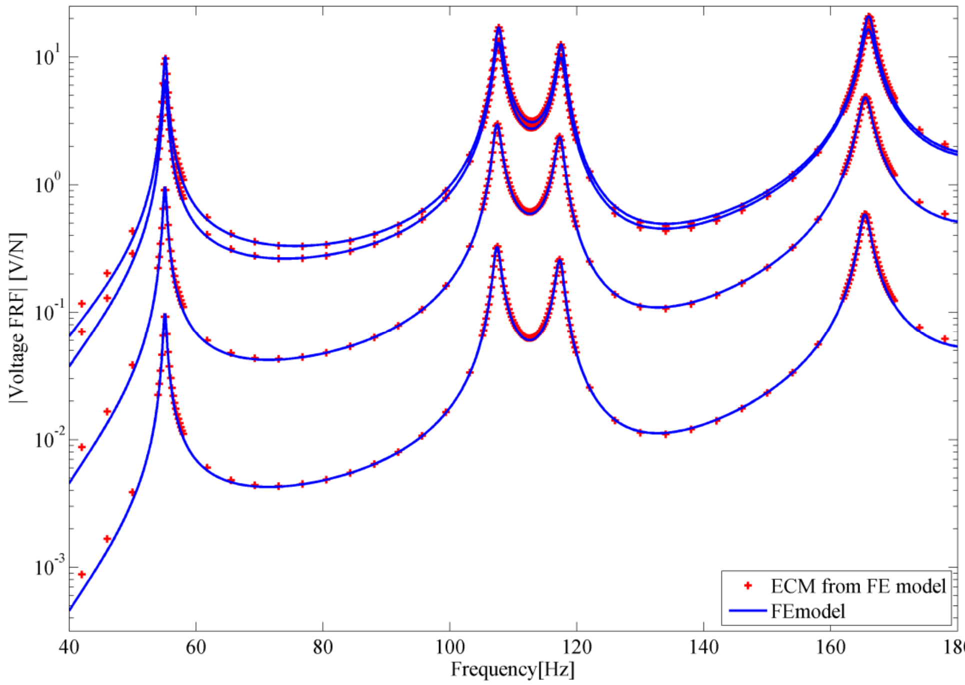

Figure 15. Comparison of voltage FRFs obtained with equivalent circuit model and FE model

Figure 16 and Figure 17 compare peak voltage and power amplitudes of the analytical and FE models at the first four short circuit natural frequencies, respectively. The results show that the equivalent circuit model accurately predicts the peak voltage and power amplitudes.

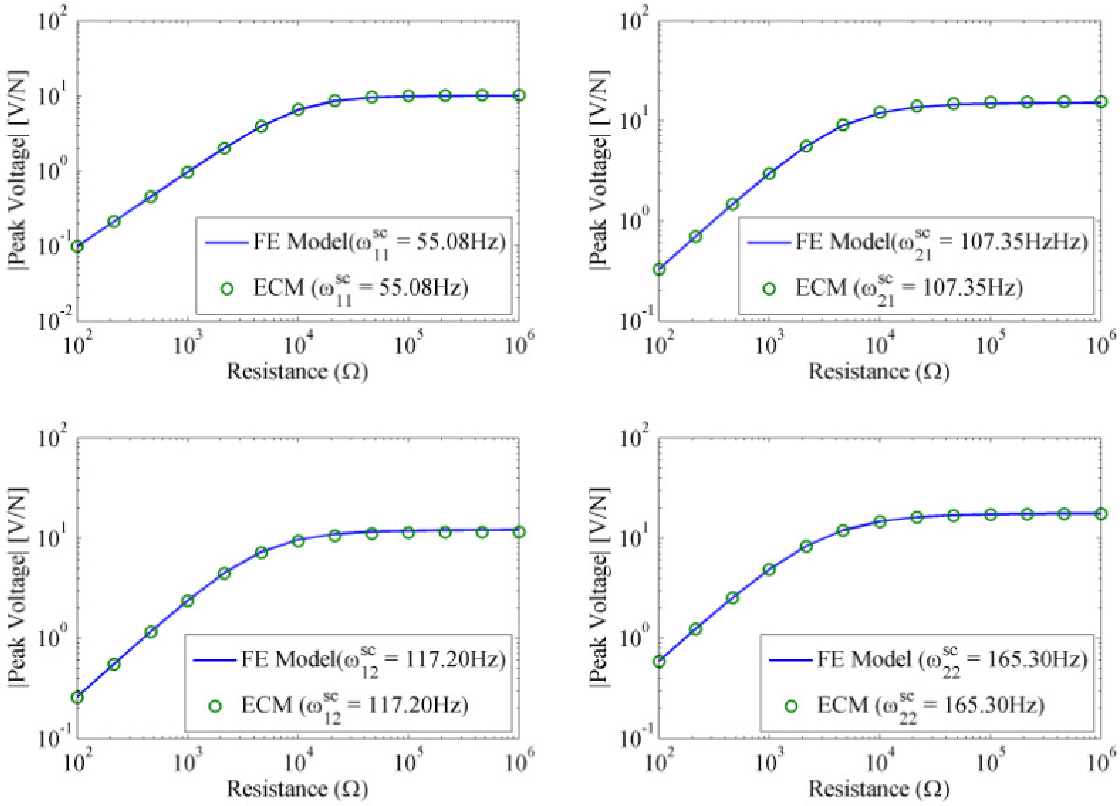

Figure 16. Comparison of voltage outputs for a wide range of resistive loads at first four short circuit natural frequencies

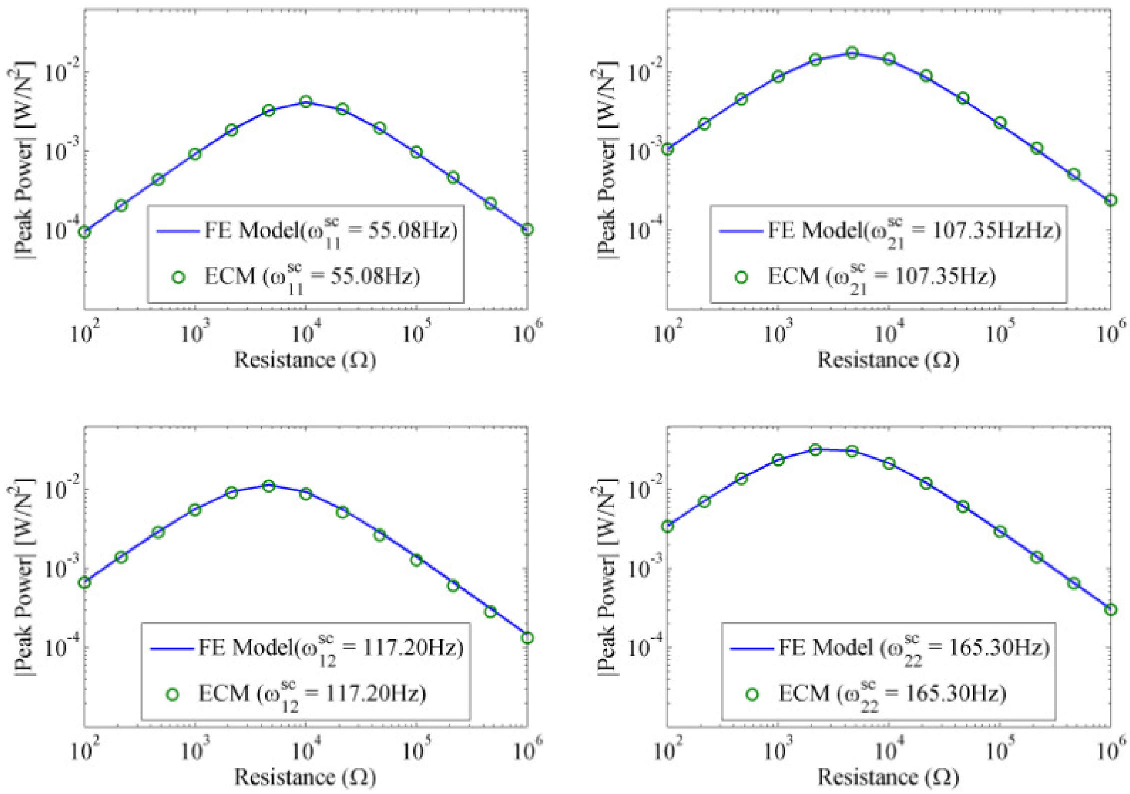

Figure 17. Comparison of power outputs for a wide range of resistive loads at first four short circuit natural frequencies

3.3.3 DC Problem Validation

For the standard DC problem, a practical energy harvesting circuit is used including a full-wave bridge rectifier and a smoothing capacitor as shown in Figure 13(b). Parameters of the equivalent circuit models are identified in Section 3.3.2.

The distributed parameter analytical model can not simulate the DC problem due to the presence of non linear circuit elements in the energy harvesting circuit. Similarly, FE model can not be used directly for modeling the energy harvester with non linear circuit elements. Therefore, the lumped parameter model suggested by Shu and Lien [46] is used to validate the voltage and power outputs obtained from the equivalent circuit model. In their study, the authors developed an analytical formulation of the rectified DC voltage output for the piezoelectric energy harvesters using a lumped-parameter approach. The closed-form expression for the steady-state voltage (V_c) of the piezoelectric patch-based harvester is given by Shu and Lien [46]as:

$$V_c = \frac{L_{mn}\omega R_l}{R_l C_p \omega + \pi/2} u_0 \quad (30)$$

where the displacement amplitude u_0 is derived in terms of the point forcing amplitude and the system parameters as

$$u_0 = \frac{F_0 \phi_{mn}(x_0, y_0)}{\left\{ \left(R_{mn}\omega + \frac{2\omega N_{mn}^2 R_l}{(C_p \omega R_l + \pi/2)^2} \right)^2 + \left(1/C_{mn} - \omega^2 L_{mn} + \frac{\omega N_{mn}^2 R_l}{C_p \omega R_l + \pi/2} \right)^2 \right\}^{\frac{1}{2}}} \quad (31)$$

To generate stable DC voltage V_c, smoothing capacitor C_e must be large enough to achieve constant DC voltage output. Ideal transformer and diodes are used in the equivalent circuit model simulations such that the results can be compared to analytical model which is based on the ideal diodes assumption. Note that analytical model is valid only in the close neighborhood of the resonance frequencies. Therefore equivalent circuit model results are compared only at natural frequencies for the DC problem.

By conducting transient analysis for the equivalent circuit model in SPICE, steady-state voltage responses are extracted for various values of resistive loads at short circuit resonance frequencies. **Error! Reference source not found.** and Figure 19 compares the SPICE simulation results with the analytical model predictions for a wide range of resistive loads for the peak DC voltage and power outputs, respectively. Again, the equivalent circuit model accurately predicts the DC voltage and power outputs. It can be also seen from the figures that there exists an optimum resistance at which the DC power output becomes maximum.

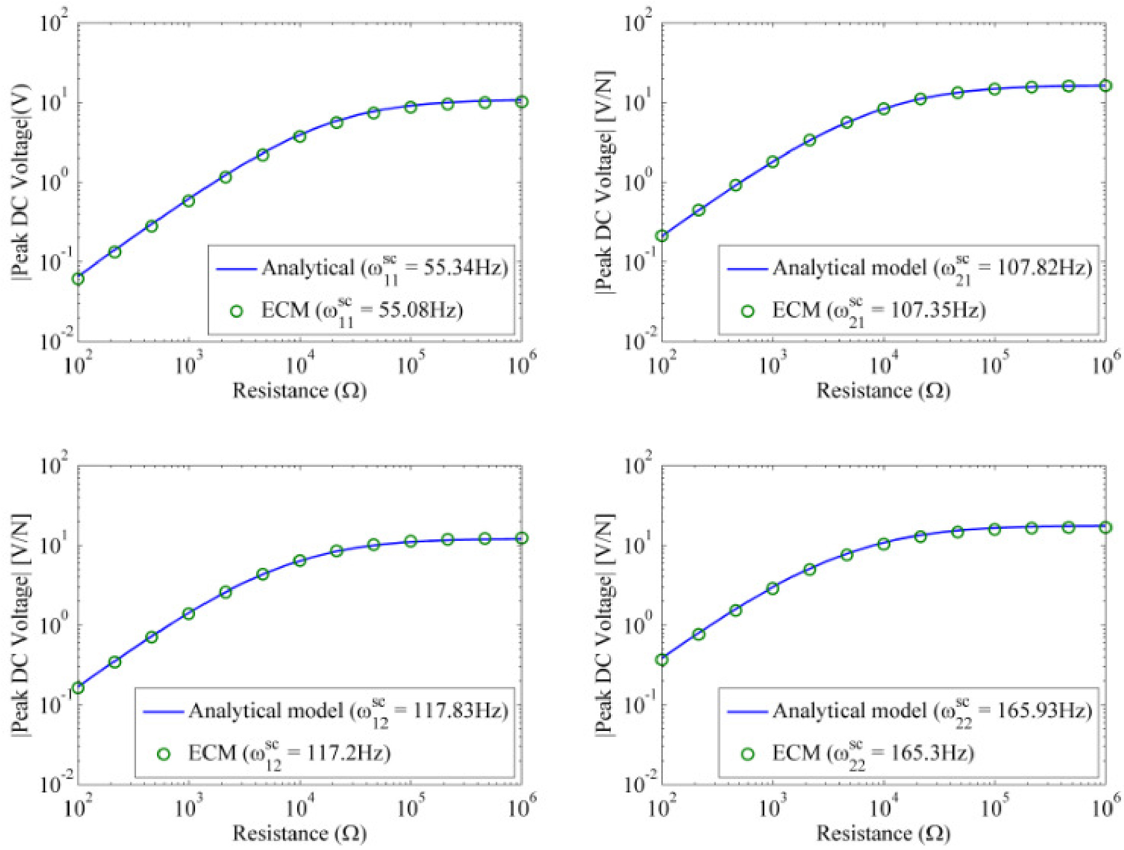

Figure 18. Comparison of voltage outputs for a wide range of resistive loads at first four short circuit natural frequencies

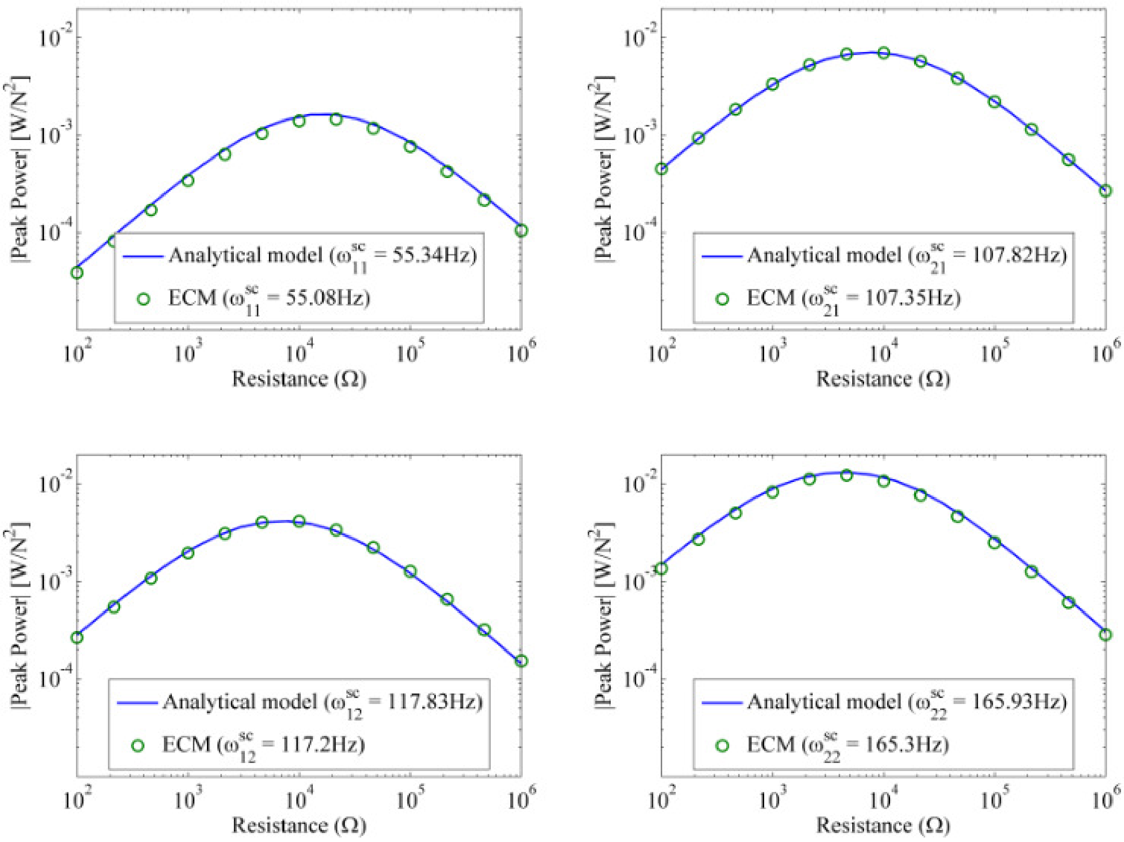

Figure 19. Comparison of power outputs for a wide range of resistive loads at first four short circuit natural frequencies

Chapter 4

ENERGY HARVESTING ON A HEAVY DUTY VEHICLE PANEL

4.1. Overview

In this chapter, electroelastic finite element (FE) modeling and numerical simulations of a patch-based piezoelectric energy harvester attached to a panel of a heavy duty vehicle are presented for different operating conditions. This chapter extends the FE modeling methodology developed in Section 2.2 to a real-life problem. Panels enclosing the vehicle cabin and the driving components of a heavy duty vehicle are mainly excited by engine forces. Engine forces are transferred through the engine mounts to the cabin mounts. The excitation forces transferred through the mounts vibrate the panels of the cabin, the steering wheel, pedals and seats [58]. In addition to the engine excitations, road disturbances transferred through the wheels and suspension system are also significant in the forced vibration of the cabin panels and components. Therefore, existing ambient mechanical energy of the cabin panels can be converted into useful electrical power. To investigate the energy harvesting potential from a heavy duty vehicle panel, numerical simulations and analysis are performed on the cabin panel in different operating conditions.

In the following section, the FE model of the heavy duty vehicle is described. Then, the details of the operational conditions and numerical simulations are given. Finally, numerical results for the structural and electrical responses are presented and discussed.

4.2. Finite Element Model

Figure 20 shows a typical heavy duty vehicle and its main components [59]. The lower part of the vehicle can be considered as the vibration source for the cabin, which contains both engine excitation and road disturbances coming from the wheels and suspension system. The upper part of the vehicle is composed of the cabin of the vehicle with back, roof and side panels. In this study, the back panel of the cabin is selected as the vibrating host structure for harvesting the vibrational energy since it is easy to attach a piezoceramic harvester patch on this panel. It is one of the most vibrating panels of the cabin [58]

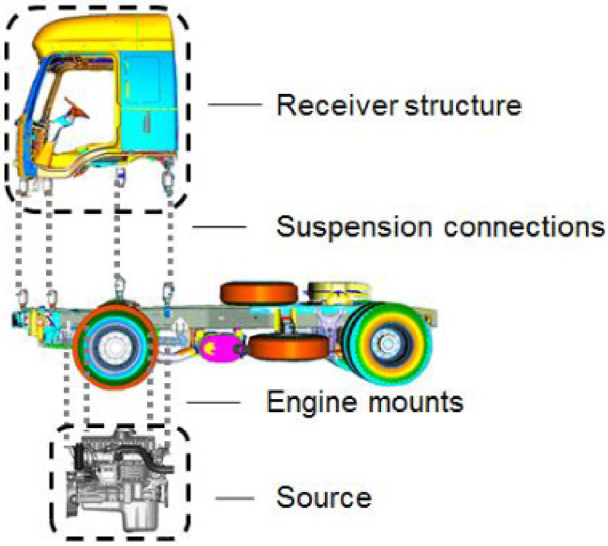

Figure 20. Source and receiver cabin structure for a typical heavy duty vehicle (mounts are the connection between receiver structure and chassis) depicted from [59]

For the numerical analysis, a detailed FE model (e.g., around 5 million degrees-of-freedom) is used including the cabin panels and suspension connections (i.e., cabin mounts) [58]. In the rest of this paper, the full FE model refers to the detailed FE model (shown in

Figure 21a) and submodel refers to the subsection of the vehicle back panel (shown in Figure 21b) where the harvester patch is attached.

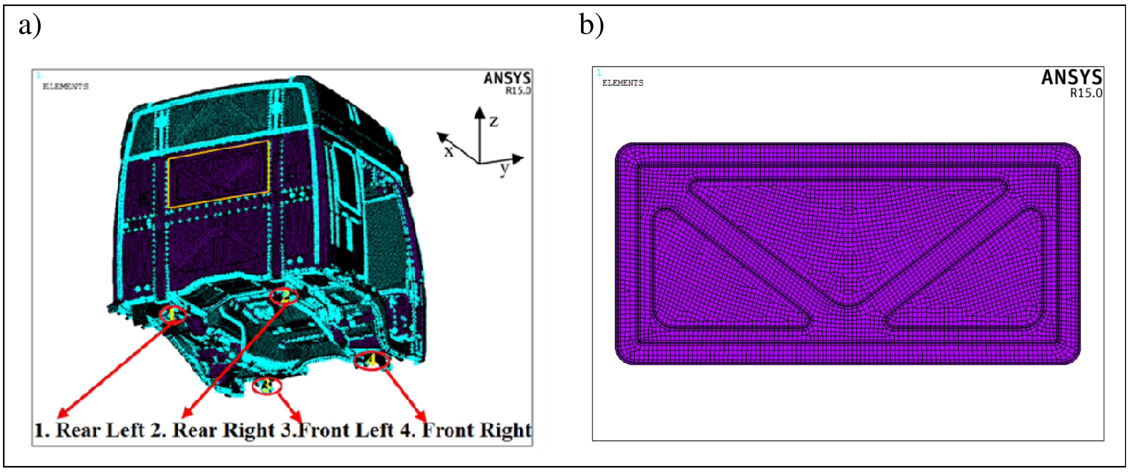

Figure 21. a) Finite element model of the cabin b) submodel of the selected section of the back panel.

The computational cost of running a piezoelectric energy harvesting analysis employing the full FE model is very high. Therefore, the results of the full FE model are used on a submodel which includes only a section of the back panel where the harvester patch is attached. Figure 21b shows the submodel and the cut boundaries, which separates the submodel from the other cabin components. By calculating displacement responses from the full FE model on the cut boundaries, numerical simulations of the submodel are performed for coupled electromechanical analysis of the harvester patch and the host structure. The full FE model is built in NASTRAN and a response analysis is conducted to extract the displacements at the cut boundaries [58]. ANSYS Mechanical APDL is used for submodelling and electromechanical modelling of the harvester connected to a resistive load. The panel is meshed with 4-node structural shell elements (SHELL181) and the piezoceramic patch is meshed with 20-node coupled field solid elements (SOLID226). Material properties of the panel and the harvester are given in Table 6.

Table 6. Geometric material and Electroelastic Properties

Property	Piezoceramic patch
Length (mm)	72.5
Width (mm)	68
Thickness (mm)	2.03
Young's Modulus (GPA)	66
Mass Density (kg/m^3)	7750
Piezoelectric Constant e31 (C/m^2)	-5.35
Piezoelectric Constant e33 (C/m^2)	15.78
Piezoelectric Constant e15 (C/m^2)	12.29
Relative Permittivity ($\varepsilon_s/\varepsilon_0$)	826.6
Free Space Permittivity ε_0 (F/m)	8.854 x 10^{-12}

The harvester and the host structure (i.e., a section the back panel as shown in Figure 21a and Figure 21b) are tied together via CEINTF command in ANSYS, which includes constraint equations relating the nodes at the bonding interfaces. To simulate the highly conductive top and bottom electrode layers of the harvester patch, the voltage degrees of freedoms (DOFs) on bottom and top surfaces are forced to be equipotential by creating a coupled DOF set for each surface. CIRCU94 piezoelectric circuit element is used for simulating the resistive load connected to the harvester patch. One end of the piezoelectric circuit element is connected to the top electrode and the other end is connected to the grounded bottom electrode to include two-way electromechanical coupling and measure the voltage output. Global 3% structural damping is used for FE simulations.

4.3. Cabin Mounts Force Identification

Identification of the operational loads during in-operation tests involves direct experimental measurements on the prototype vehicle. The force identification steps include (i) operational acceleration measurements on the cabin mounts (e.g. run-up, run-down) on the road or on a chassis dyno and (ii) measurement of the frequency response functions (FRF's) from excitation tests (e.g., hammer impact tests, shaker tests). Matrix inversion is a force identification technique that is used to predict the forces acting on the certain locations of the structure based on the operational accelerations and frequency response functions (FRFs) measured during the experiments. Prior to this study, the operational loads acting on the four cabin mounts (see Figure 21a for the location of the cabin mounts) were identified by using this matrix inversion technique based on experimental measurements [59]. For instance, for n number of the cabin mounts, the acceleration response and FRF matrix can be expressed as follows:

$$\begin{Bmatrix} \ddot{x}_{11} \\ \vdots \\ \ddot{x}_{nn} \end{Bmatrix} = \begin{bmatrix} \mathrm{G}_{11} & \cdots & \mathrm{G}_{1\mathrm{n}} \\ \vdots & \ddots & \vdots \\ G_{n1} & \cdots & G_{nn} \end{bmatrix} \begin{Bmatrix} f_1 \\ \vdots \\ f_n \end{Bmatrix} \quad (32)$$

where f_i is the internal forces acting on the active side of the cabin mount i, $\ddot{\mathrm{x}}_1$ is the operational acceleration at the passive side of the cabin mount i, G_{ij} is the accelerance FRF between the passive side of the cabin mount i and the active side of the cabin mount j, where $\forall i, j \in \{1, \ldots, n\}$. For linearly independent n number of cabin mounts and assuming that FRF matrix is invertible, the forces can be obtained by inverting the FRF matrix. Once these excitation forces are calculated, they can be applied at the mount locations to predict the response of the structure under operating conditions.

4.4. Vibration Modes of the Back Panel and the Harvester Location

Modal analysis of the cabin results in more than 100 resonant modes between 0 and 100 Hz due to the complexity of the structure. Figure 22 demonstrates four selected undamped natural frequencies and corresponding mode shapes of the back side of the cabin. The first undamped natural frequency of the back panel is 26.6 Hz, where the mode shape of this resonance has maximum deflection in the center of the panel. In the other vibration modes, the maximum deflection occurs in different locations leading to several in-phase and out-phase displacement regions over the back panel surface. The nodal lines of the vibration modes, where the sign of displacement change, must be examined carefully when attaching the harvester patch to the host structure. Since electrical output of the harvester patch is greatly dependent on the homogenous strain distribution over the surface of the host plate, improper locations of harvester patch may cause cancellation in electrical outputs and thus decrease the performance of harvester [60]. Figure 23 displays the piezoceramic patch attached to the surface of the host structure. Strain distribution observations reveal that 26.6 Hz and 54.45 Hz modes of the back panel are effective at the location where the piezoceramic patch is attached.

Mode 1: 26.64Hz

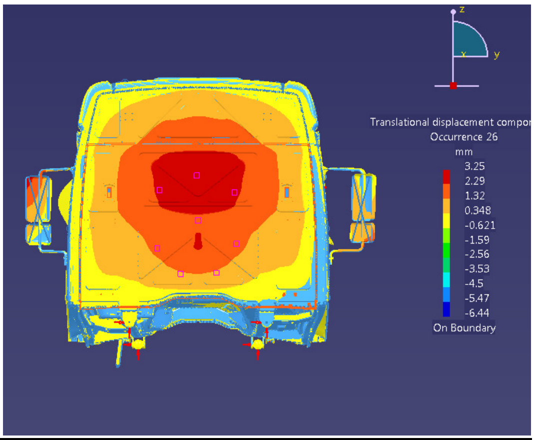

Mode 2: 42.78Hz

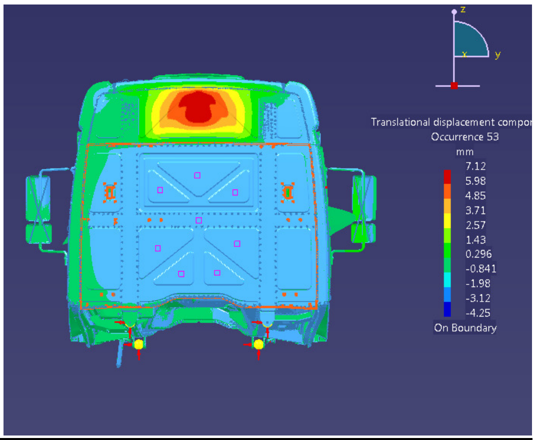

Mode 3: 48.54Hz

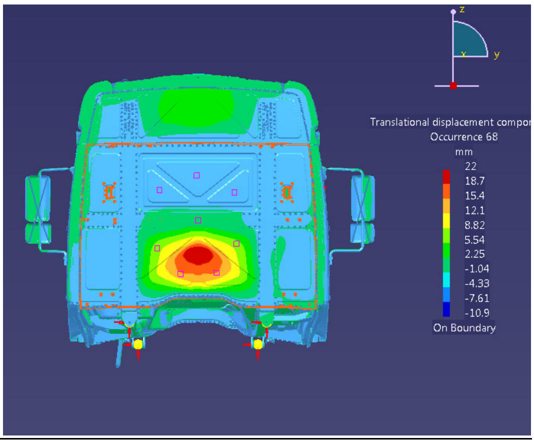

Mode 4: 54.45Hz

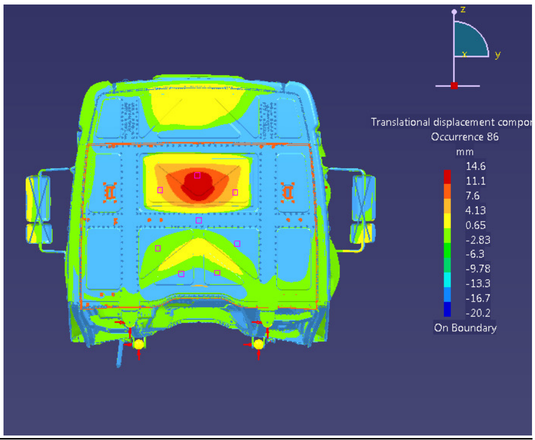

Figure 22. . Natural frequencies and corresponding mode shapes of back side of the cabin.

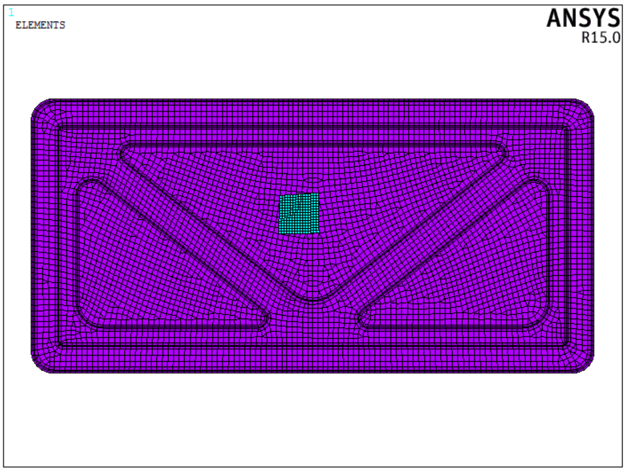

Figure 23. Harvester location on the host structure

The host structure is excited by the forces applied to four of the cabin mounts in three directions (*i.e.* x, y, z directions). The locations and names of these mounts are displayed in Figure 21a. In order to verify the submodeling predictions, displacement FRF (in mm/N) along the x-direction between vibration response at the center of the patch and the force acting along the z-direction of the rear right mount is computed for both the full FE model and the submodel. The comparison of these displacement FRFs are shown in Figure 24. The submodel results of the back panel agree well with the displacement response predictions of the full FE model.

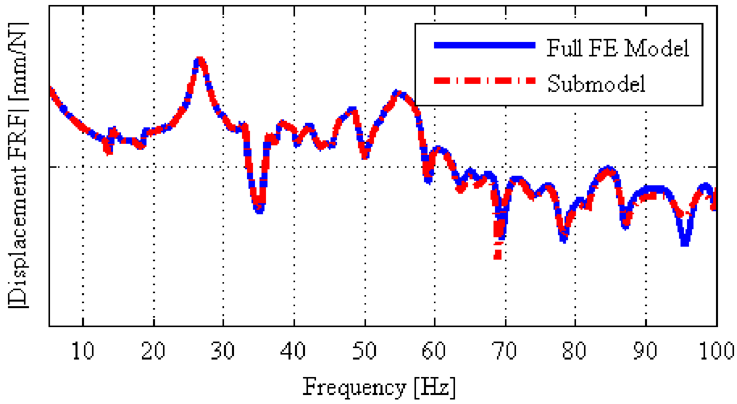

Figure 24. Comparison of displacement FRF (mm/N) between full FE model and submodel.

4.5. Voltage and Power Output Results

In this section, patch-based piezoelectric energy harvesting on the back panel of the cabin is investigated at stationary and moving conditions of the heavy duty vehicle. The stationary condition of the heavy duty vehicle is the case in which the engine is running and the vehicle is not moving. This is a typical operation of heavy duty vehicles which are used for such activities as surveillance and concrete mixing. The second condition is the moving condition of the vehicle, which generally covers a wide range of regular operations of heavy duty vehicles used for transportation. Note that, the forces at the cabin mounts are given as input for the two operating conditions, and structural and electrical responses are obtained using the submodel and presented for each operating condition.

Table 7. Resistive Loads

Resistance Order	Resistance Value (kΩ)	Resistance Order	Resistance Value (kΩ)
1	0.10	9	71.96
2	0.22	10	163.78
3	0.51	11	372.75
4	1.17	12	848.34
5	2.68	13	1930.70
6	6.10	14	4393. 97
7	13.89	15	10000
8	31.62		

The voltage output of the harvester patch is monitored by connecting a resistive load to the harvester patch attached on the back panel of the vehicle. Figure 25a shows the displacement response (mm) and Figure 25b shows the voltage output (V) for the two operation conditions, in which the load resistance is used as 10 MΩ (close to open-circuit conditions). As can be observed from Figure 25, in the moving condition, the higher voltage amplitudes can be generated in a wide frequency range. To explore the voltage output for a wide range of resistive loads, resistor sweep test is carried out. A set of resistors listed in Table 7 is used ranging from near to short-circuit conditions (10^2 Ω) to open-circuit conditions (10^7 Ω).

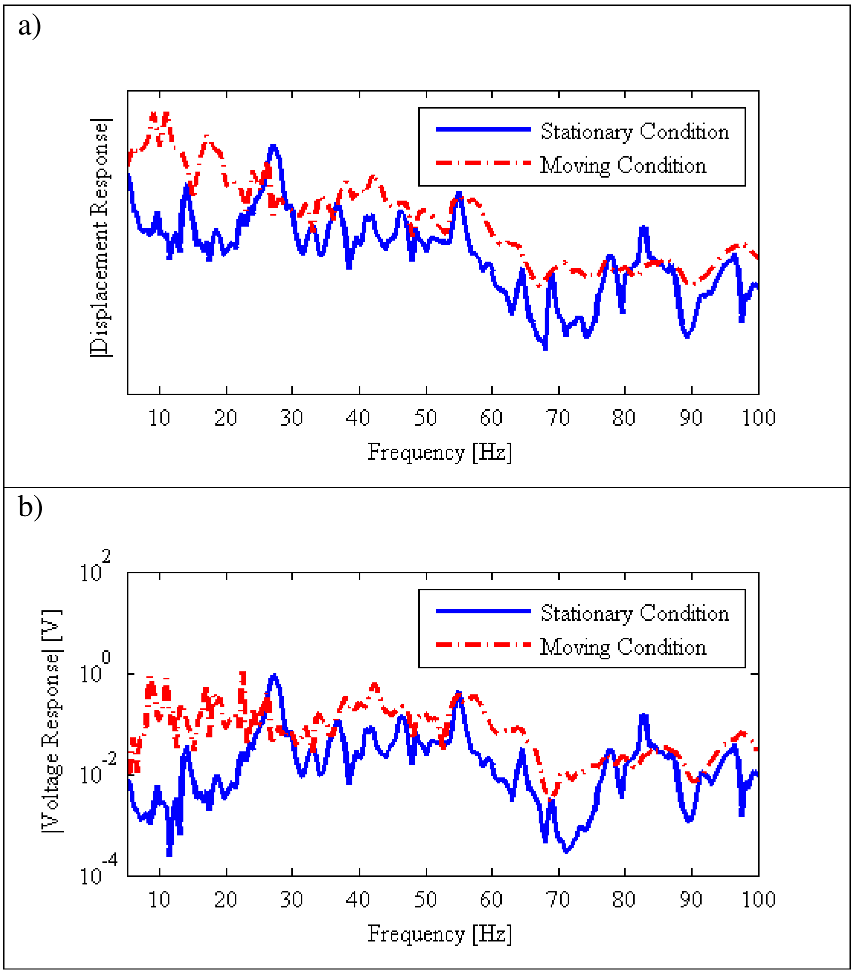

Figure 25. a) Displacement response b) Voltage output for two case studies at open-circuit condition

Voltage output increases up to 0.42 V in moving condition and 0.9 V in stationary condition for the selected first vibration mode (at 26.6 Hz). Each load resistance leads to different voltage output. At the open-circuit resonance frequencies of 26.6 Hz and 54.45 Hz, the vibration response and voltage output are higher in stationary condition as compared to moving condition. This result implies that the back panel is more excited at 26.6 Hz and 54.45 Hz for the case of stationary condition. After that, electrical power output across the resistive load is calculated with ($P = V^2 / R$) and the peak power amplitudes at 26.6 Hz and 54.45 Hz are identified for each resistor. Figure 26a and Figure 26b present the peak power amplitudes for both of two operating conditions at 26.6 Hz and 54.45 Hz frequencies, respectively. As expected, an optimal resistive load exists where the power output reaches the maximum value. The optimal resistive load and the maximum power output differ at each resonance frequency.

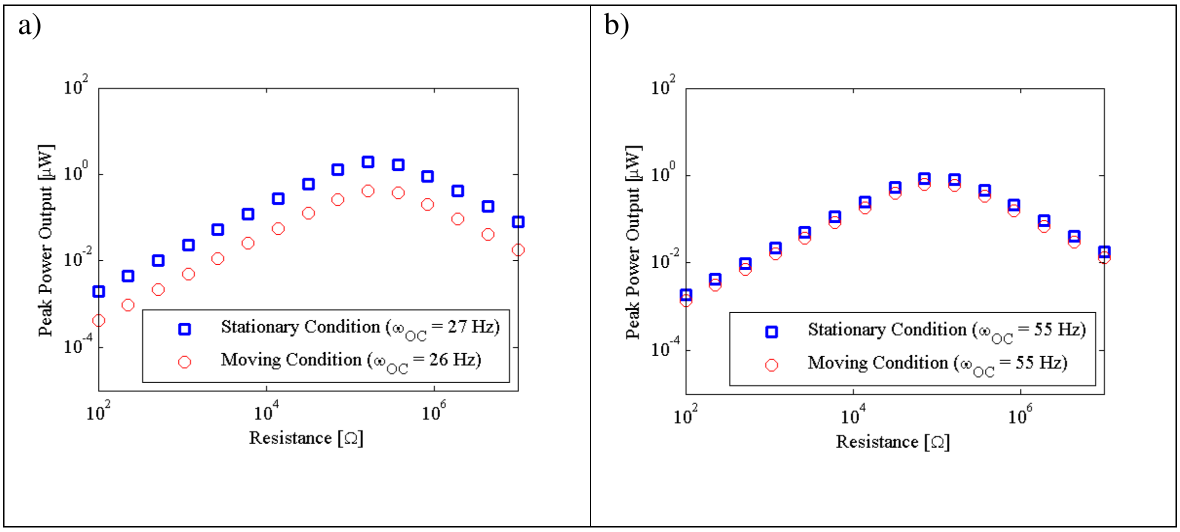

Figure 26. Peak power vs. resistive load for open circuit resonance frequencies of a) at 26.6 Hz mode and b) at 54.45 Hz mode in two different operating conditions

The maximum peak power amplitude is extracted up to 2 μW for the stationary condition and 0.5 μW for the moving condition of the vehicle at 26.6 Hz vibration mode of back panel. In the second selected vibration mode (54.45 Hz), the maximum peak power can be generated up to 0.9 μW for the stationary and 0.65 μW for the moving condition. Note that these power values are calculated for a finite set of resistors and more accurate results can be calculated by fine tuning the resistive load.

FE model simulations show that it is convenient to use the patch harvesters attached on a plate like structure (i.e., back panel of the vehicle cabin) for vibrational energy harvesting and the power outputs are in μW level for this specific application.

Chapter 5

SUMMARY AND CONCLUSIONS

Reduction of the power requirement of small electronic components made it possible to build self powered sensors by harvesting the ambient vibration energy. Among several harvesting mechanisms to convert ambient vibration to electrical energy, piezoelectric energy harvesting received the greatest attention by researchers due to their larger power densities. Considering the advancements and the needs in piezoelectric energy harvesting, this thesis presents a methodology for equivalent circuit modeling and analysis of a patch based energy harvester integrated to a thin plate using a coupled electroelastic FE model. The methodology presented provide a systematic way to investigate the voltage and power output of patch based harvesters and provides the opportunity to analyze real life implementations of energy harvesters. This thesis is divided into 5 main chapters. In Chapter 1, an introduction about the piezo electric energy harvesting was given and the relevant literature was reviewed. Chapter 2 described the finite element analysis procedure used in the modeling of the patch based harvester that was attached to the plate structure. The energy harvesting circuit was represented by a single resistive load connected to the top and bottom electrodes of the piezoceramic patch and full conductivity of the electrodes were included in the FE model. FRFs of the voltage and power outputs of the energy harvester were obtained and validated with analytical distributed parameter model derived by Aridogan et al. [21]. Agreement between analytical and FE model results showed that

FE model accurately predicted natural frequencies, peak voltage and peak power amplitudes. It was observed from both analytical and FE models that voltage amplitudes at natural frequencies increased with increasing resistive load and remained constant after open circuit condition was achieved.

In Chapter 3, equivalent circuit representation of a patch based energy harvester was developed and a practical energy harvesting circuit with non-linear circuit elements was included in the model. Equivalent parameters of the circuit model were determined using the FE model developed in Chapter 2. Equivalent circuit model of the harvester was constructed in SPICE software and simulation results were verified using two numerical examples with different energy harvesting circuit configurations. The first example included a single resistive load whereas the second example included a full-wave bridge rectifier followed by a smoothing capacitor. The first numerical problem was referred as AC problem and peak voltage and power outputs for several resistive loads were compared with the analytical model derived by Aridogan et al. [21]. It was shown that the equivalent circuit model accurately predicted the peak voltage and power amplitudes for the AC problem. In addition, voltage FRFs of the equivalent circuit model and the analytical model were compared and good agreement was observed for a frequency range covering off-resonance frequencies as well. The second numerical problem was referred as DC problem and validated using the lumped parameter model suggested by Shu and Lien [46]. The equivalent circuit model accurately predicted the DC voltage and power outputs at natural frequencies. Since the lumped parameter model was not valid for off-resonance frequencies, power and voltage outputs were compared only at natural frequencies.

In Chapter 4, the FE modeling technique developed in Chapter 2 was extended to a real life application. Numerical simulations of a patch-based piezoelectric energy harvester attached to a panel of a heavy duty vehicle were presented. The vibration response of the panel as well as the voltage output of the harvester patch under operating conditions was simulated using the forces obtained from experimental measurements on the heavy duty vehicle. Two different operating conditions of the heavy duty vehicle were used: stationary and moving on a test track while the engine was running. Using the excitation forces in the FE simulations, the electrical power generation of the harvester patch was predicted for a wide range of resistive loads. Electrical power outputs were then presented for short-circuit and open-circuit conditions. The numerical results showed that the use of a harvester patch attached on a panel of a heavy duty vehicle generated reasonably good electrical power outputs.

For future studies, parameters of the equivalent circuit model can be directly obtained from the analytical model derived by Aridogan et al. [21] following the procedures suggested by Elvin and Elvin [52] or Yang and Tang [51]. Rectified electrical outputs of the equivalent circuit model obtained from FEA can be compared with the ones obtained from the analytical model and rectified outputs can be also verified at off-resonance frequencies. In addition, the real life application presented in chapter 4 can be further investigated by including a practical energy harvesting circuit in the simulation and also can be validated with some experimental studies. For further improvement in the harvested energy, shape and/or location optimization study can be conducted on the patch attached on the cabin of the heavy duty vehicle based on the study of Lee and Youn [61] and power output of the harvester can be increased. In energy harvesting literature, recent research efforts are focused on non linear energy harvesters to improve the electrical outputs under broadband excitations. In addition, researchers are heading towards other energy sources than harmonic vibrations, such as wind and water flow energy, air and structure-borne waves and impulse type kinetic energy [62].

BIBLIOGRAPHY

1. Naruse, Y., et al., *Electrostatic micro power generation from low-frequency vibration such as human motion.* Journal of Micromechanics and Microengineering, 2009. **19**(9).
2. Torres, E.O. and G.A. Rincón-Mora, *A 0.7-μm biCMOS electrostatic energy-harvesting system IC.* IEEE Journal of Solid-State Circuits, 2010. **45**(2): p. 483-496.
3. Beeby, S.P., et al., *A micro electromagnetic generator for vibration energy harvesting.* Journal of Micromechanics and Microengineering, 2007. **17**(7): p. 1257-1265.
4. Yang, B., et al., *Electromagnetic energy harvesting from vibrations of multiple frequencies.* Journal of Micromechanics and Microengineering, 2009. **19**(3): p. 035001.
5. Beeby, S.P., M.J. Tudor, and N.M. White, *Energy harvesting vibration sources for microsystems applications.* Measurement Science and Technology, 2006. **17**(12): p. R175-R195.
6. Anton, S.R. and H.A. Sodano, *A review of power harvesting using piezoelectric materials (2003-2006).* Smart Materials and Structures, 2007. **16**(3): p. R1-R21.
7. El-hami, M., et al., *Design and fabrication of a new vibration-based electromechanical power generator.* Sensors and Actuators a-Physical, 2001. **92**(1-3): p. 335-342.
8. Sasaki, K., et al., *Vibration-based automatic power-generation system.* Microsystem Technologies-Micro-and Nanosystems-Information Storage and Processing Systems, 2005. **11**(8-10): p. 965-969.
9. Amirtharajah, R. and A.P. Chandrakasan, *Self-powered signal processing using vibration-based power generation.* Ieee Journal of Solid-State Circuits, 1998. **33**(5): p. 687-695.
10. Miyazaki, M., et al., *Electric-energy generation through variable-capacitive resonator for power-free LSI.* Ieice Transactions on Electronics, 2004. **E87c**(4): p. 549-555.
11. Cook-Chennault, K.A., N. Thambi, and A.M. Sastry, *Powering MEMS portable devices - a review of non-regenerative and regenerative power supply systems with special emphasis on piezoelectric energy harvesting systems.* Smart Materials and Structures, 2008. **17**(4).

12. Erturk, A. and D.J. Inman, *Piezoelectric energy harvesting*. 2011: John Wiley & Sons.
13. Choi, W.J., et al., *Energy harvesting MEMS device based on thin film piezoelectric cantilevers.* Journal of Electroceramics, 2006. **17**(2-4): p. 543-548.
14. Jeon, Y.B., et al., *MEMS power generator with transverse mode thin film PZT.* Sensors and Actuators a-Physical, 2005. **122**(1): p. 16-22.
15. Mitcheson, P.D., et al., *MEMS electrostatic micropower generator for low frequency operation.* Sensors and Actuators a-Physical, 2004. **115**(2-3): p. 523-529.
16. Roundy, S. and P.K. Wright, *A piezoelectric vibration based generator for wireless electronics.* Smart Materials & Structures, 2004. **13**(5): p. 1131-1142.
17. Roundy, S., P.K. Wright, and J. Rabaey, *A study of low level vibrations as a power source for wireless sensor nodes.* Computer Communications, 2003. **26**(11): p. 1131-1144.
18. Ajitsaria, J., et al., *Modeling and analysis of a bimorph piezoelectric cantilever beam for voltage generation.* Smart Materials & Structures, 2007. **16**(2): p. 447-454.
19. Erturk, A. and D.J. Inman, *A distributed parameter electromechanical model for cantilevered piezoelectric energy harvesters.* Journal of Vibration and Acoustics-Transactions of the Asme, 2008. **130**(4).
20. Erturk, A. and D.J. Inman, *An experimentally validated bimorph cantilever model for piezoelectric energy harvesting from base excitations.* Smart Materials and Structures, 2009. **18**(2): p. 025009.
21. Aridogan, U., I. Basdogan, and A. Erturk, *Analytical modeling and experimental validation of a structurally integrated piezoelectric energy harvester on a thin plate.* Smart Materials and Structures, 2014. **23**(4).
22. Lee, S., B.D. Youn, and M. Giraud, *Designing Energy Harvesting Skin Structure Utilizing Outdoor Unit Vibration.* Proceedings of the Asme International Design Engineering Technical Conferences and Computers and Information in Engineering Conference, Detc 2010, Vol 4, 2010: p. 713-723.
23. Aridogan, U., I. Basdogan, and A. Erturk, *Multiple patch-based broadband piezoelectric energy harvesting on plate-based structures.* Journal of Intelligent Material Systems and Structures, 2014. **25**(14): p. 1664-1680.
24. Erturk, A. and D.J. Inman, *Issues in mathematical modeling of piezoelectric energy harvesters.* Smart Materials & Structures, 2008. **17**(6).
25. Williams, C.B. and R.B. Yates, *Analysis of a micro-electric generator for microsystems.* Sensors and Actuators a-Physical, 1996. **52**(1-3): p. 8-11.
26. duToit, N.E., B.L. Wardle, and S.G. Kim, *Design considerations for MEMS-scale piezoelectric mechanical vibration energy harvesters.* Integrated Ferroelectrics, 2005. **71**: p. 121-160.

27. Erturk, A. and D.J. Inman, *On Mechanical Modeling of Cantilevered Piezoelectric Vibration Energy Harvesters.* Journal of Intelligent Material Systems and Structures, 2008. **19**(11): p. 1311-1325.
28. Dutoit, N.E. and B.L. Wardle, *Experimental verification of models for microfabricated piezoelectric vibration energy harvesters.* Aiaa Journal, 2007. **45**(5): p. 1126-1137.
29. Lin, J.H., et al., *Modeling and simulation of piezoelectric MEMS energy harvesting device.* Integrated Ferroelectrics, 2007. **95**: p. 128-141.
30. Chen, S.N., G.J. Wang, and M.C. Chien, *Analytical modeling of piezoelectric vibration-induced micro power generator.* Mechatronics, 2006. **16**(7): p. 379-387.
31. Lu, F., H.P. Lee, and S.P. Lim, *Modeling and analysis of micro piezoelectric power generators for micro-electromechanical-systems applications.* Smart Materials & Structures, 2004. **13**(1): p. 57-63.
32. Sodano, H.A., G. Park, and D.J. Inman, *Estimation of electric charge output for piezoelectric energy harvesting.* Strain, 2004. **40**(2): p. 49-58.
33. Shahruz, S.M., *Design of mechanical band-pass filters for energy scavenging: Multi-degree-of-freedom models.* Journal of Vibration and Control, 2008. **14**(5): p. 753-768.
34. Leland, E.S. and P.K. Wright, *Resonance tuning of piezoelectric vibration energy scavenging generators using compressive axial preload.* Smart Materials and Structures, 2006. **15**(5): p. 1413.
35. Hu, Y., H. Xue, and H. Hu, *A piezoelectric power harvester with adjustable frequency through axial preloads.* Smart Materials and Structures, 2007. **16**(5): p. 1961.
36. Wu, X., et al., *A frequency adjustable vibration energy harvester.* Proceedings of PowerMEMS, 2008: p. 245-248.
37. Challa, V.R., et al., *A vibration energy harvesting device with bidirectional resonance frequency tunability.* Smart Materials and Structures, 2008. **17**(1): p. 015035.
38. Erturk, A., J. Hoffmann, and D.J. Inman, *A piezomagnetoelastic structure for broadband vibration energy harvesting.* Applied Physics Letters, 2009. **94**(25): p. 254102.
39. Peters, C., et al., *A closed-loop wide-range tunable mechanical resonator for energy harvesting systems.* Journal of Micromechanics and Microengineering, 2009. **19**(9): p. 094004.
40. De Marqui, C., A. Erturk, and D.J. Inman, *An electromechanical finite element model for piezoelectric energy harvester plates.* Journal of Sound and Vibration, 2009. **327**(1-2): p. 9-25.

41. De Marqui, C., A. Erturk, and D.J. Inman, *Piezoaeroelastic Modeling and Analysis of a Generator Wing with Continuous and Segmented Electrodes.* Journal of Intelligent Material Systems and Structures, 2010. **21**(10): p. 983-993.
42. De Marqui, C., et al., *Modeling and Analysis of Piezoelectric Energy Harvesting From Aeroelastic Vibrations Using the Doublet-Lattice Method.* Journal of Vibration and Acoustics-Transactions of the Asme, 2011. **133**(1).
43. Rupp, C.J., et al., *Design of Piezoelectric Energy Harvesting Systems: A Topology Optimization Approach Based on Multilayer Plates and Shells.* Journal of Intelligent Material Systems and Structures, 2009. **20**(16): p. 1923-1939.
44. Harne, R.L., *Concurrent attenuation of, and energy harvesting from, surface vibrations: experimental verification and model validation.* Smart Materials and Structures, 2012. **21**(3): p. 035016.
45. Harne, R.L., *Development and testing of a dynamic absorber with corrugated piezoelectric spring for vibration control and energy harvesting applications.* Mechanical Systems and Signal Processing, 2013. **36**(2): p. 604-617.
46. Shu, Y.C. and I.C. Lien, *Analysis of power output for piezoelectric energy harvesting systems.* Smart Materials & Structures, 2006. **15**(6): p. 1499-1512.
47. Ottman, G.K., et al., *Adaptive piezoelectric energy harvesting circuit for wireless remote power supply.* Ieee Transactions on Power Electronics, 2002. **17**(5): p. 669-676.
48. Guyomar, D., et al., *Toward energy harvesting using active materials and conversion improvement by nonlinear processing.* Ieee Transactions on Ultrasonics Ferroelectrics and Frequency Control, 2005. **52**(4): p. 584-595.
49. Guyomar, D., et al., *Piezoelectric energy harvesting using a synchronized switch technique.* Smart Materials for Engineering and Biomedical Applications, Proceedings, 2004: p. 17-26.
50. Shu, Y.C., I.C. Lien, and W.J. Wu, *An improved analysis of the SSHI interface in piezoelectric energy harvesting.* Smart Materials & Structures, 2007. **16**(6): p. 2253-2264.
51. Yang, Y.W. and L.H. Tang, *Equivalent Circuit Modeling of Piezoelectric Energy Harvesters.* Journal of Intelligent Material Systems and Structures, 2009. **20**(18): p. 2223-2235.
52. Elvin, N.G. and A.A. Elvin, *A General Equivalent Circuit Model for Piezoelectric Generators.* Journal of Intelligent Material Systems and Structures, 2009. **20**(1): p. 3-9.
53. Elvin, N.G. and A.A. Elvin, *A Coupled Finite Element-Circuit Simulation Model for Analyzing Piezoelectric Energy Generators.* Journal of Intelligent Material Systems and Structures, 2009. **20**(5): p. 587-595.

54. *IEEE Standard on piezoelectricity.* Ieee Transactions on Ultrasonics Ferroelectrics and Frequency Control, 1996. **43**(5): p. A1-A54.
55. Engineering Fundamentals, I.w.e.c.
56. Ansys, I., ANSYS Mechanical APDL and Mechanical Applications Element Reference, 2013.
57. Jones, T.B. and N.G. Nenadic., *Electromechanics and MEMS*. 2013: Cambridge University Press.
58. Yenerer, H., et al. *Vibro-accoustic analysis of a heavy duty truck cabin*. in *Proceedings of the 12th Biennial Conference on Engineering Systems Design and Analysis*. 2014. Copenhagen, Denmark.
59. Stan, A., et al. *Experimental transfer path analysis for a heavy duty truck*. in *Proceedings of the 12th Biennial Conference on Engineering Systems Design and Analysis*. 2014.
60. Aridogan, U., I. Basdogan, and A. Erturk. *Multiple Patch-Based Piezoelectric Energy Harvesting From Multiple Vibration Modes of Thin Plates*. in *ASME 2013 Conference on Smart Materials, Adaptive Structures and Intelligent Systems*. 2013. American Society of Mechanical Engineers.
61. Lee, S. and B.D. Youn, *A New Piezoelectric Energy Harvesting Design Concept: Multimodal Energy Harvesting Skin.* Ieee Transactions on Ultrasonics Ferroelectrics and Frequency Control, 2011. **58**(3): p. 629-645.
62. Elvin, N. and A. Erturk, *Advances in energy harvesting methods*. 2013: Springer Science & Business Media.